Title
Repetitive and Iterative Learning Control for Power Converter and Precision Motion Control

Author
Teng, Kuo-Tai

Publication Date
2014

Peer reviewed|Thesis/dissertation

University of California
Los Angeles

Repetitive and Iterative Learning Control for Power Converter and Precision Motion Control

A dissertation submitted in partial satisfaction
of the requirements for the degree
Doctor of Philosophy in Mechanical Engineering

by

Kuo-Tai Teng

2014

Abstract of the Dissertation

Repetitive and Iterative Learning Control for Power Converter and Precision Motion Control

by

Kuo-Tai Teng

Doctor of Philosophy in Mechanical Engineering

University of California, Los Angeles, 2014

Professor Tsu-Chin Tsao, Chair

This thesis develops learning control algorithms for power converters and precision motion control. The repetitive control is designed for power converters to provide zero steady state error and harmonic compensation. A model-based iterative learning control is designed for linear motor to track given reference profile with sub-micron RMS error.

The objective of the control design for power converters is to compensate harmonic distortions in the AC side to enhance power factor of the power converter. For power inverter, implementations focus on compensating harmonic distortions in the output AC voltage; For power rectifier, the objective is to compensate harmonic distortions in the input AC current.

In order to compensate harmonics for power converters, the prototype repetitive control [TTC89] is first being applied to power inverter in fixed frame. However, the power rectifier is not a linear system. To linearize the system at a more meaningful equilibrium point, a D-Q transformation is applied. But the original single-input single-output system become multi-input multi-output system in D-Q rotating frame, the famous prototype repetitive control design mythology can not be applied directly.

Repetitive control for multi-input multi-output system is developed for the control of power converters in D-Q rotating frame. The coupled dynamics in the multi-input multi-output system is first decoupled by utilizing the Smith-McMillan decomposition. Then the prototype repetitive control design is applied to the decoupled single-input single-output system.

In the precision motion control, model-based iterative learning control is proposed to achieve sub-micron RMS tracking error. The learning filter in iterative learning control determines the performance in terms of convergence rate and converged error. The ideal learning filter is the inverse of the system being learned. For non-minimum phase system, direct system inversion would result in an unstable filter.

In this thesis, a data-based dynamic inversion method in frequency domain is proposed. Different inversion filter was investigated in the thesis including Zero-Phase-Error-Tracking-Controller (ZPETC), Zero-Magnitude-Error-Tacking-Controller (ZMETC), Direct inversion, data-based phase compensator, and the proposed data-based frequency domain inversion.

The dissertation of Kuo-Tai Teng is approved.

Lieven Vandenberghe

Tetsuya Iwasaki

James S. Gibson

Tsu-Chin Tsao, Committee Chair

University of California, Los Angeles

2014

To my family,

for being immeasurably supportive

Table of Contents

List of Figures

List of Tables

Acknowledgments

First, and most importantly, I would like to express my deepest gratitude to my advisor, Professor Tsu-Chin Tsao, for his excellent guidance, caring, patience, and providing me with an excellent atmosphere for doing research. His amazing creativity and wisdom has guided me throughout the ups and downs of my academic career. I would never have been able to finish my dissertation without his guidance.

I would also like to thank Professor Lieven Vandenberghe, Professor Tetsuya Iwasaki, and Professor Steve Gibson for being excellent committee members.

The labmates in Mechatronics and Controls Laboratory also played a vital role in my PhD life. I am extremely thankful for my lab mates, Kevin Chu, Jason Wilson, Chris Lim, Herrick Chang, Stephen Prince, David Leuong, Chris Kang, Yen-Chi Chang, James Simonelli, Sandeep Rai, and Grant Cavalier. Its been a great asset being able to bounce idea back and forth among all of them. I would especially like to thank Kevin for being extremely helpful in guiding me in the first half of my PhD life. I would also like to thank Chris Kang for being a good neighbour who pop-out jokes while I was stuck in research. As for "team microgrid", I would like to thank Sandeep for brainstorming on the power electronic ideas with me all the time.

My parents have been extremely supportive and loving. I have to thank my parents for instilling in me the importance of learning. They sacrificed so much to give me and my siblings the best environment to grow and study. Without their selfless love, I would not be where I am today.

Finally, I would like to thank my wife, Pei-Fang, for her support, encouragement, and unwavering love in these past years.

Vita

2007	B.S. (Mechanical Engineering), National Taiwan University, Taipei, Taiwan
2010–2013	Teaching Assistant, Mechanical and Aerospace Engineering Department, University of California - Los Angeles, Los Angeles, California.
2010–2014	Research Assistant, Mechanical and Aerospace Engineering Department, University of California - Los Angeles, Los Angeles, California.
2012	M.S. (Mechanical Engineering), University of California - Los Angeles, Los Angeles, California.

Publications

K.-T. Teng, K.-C, Chang, Y.-Y. Chen, and T.-C. Tsao, "Respiration induced liver motion tracking control for high intensity focused ultrasound treatment", In Advanced Intelligent Mechatronics (AIM), Jul. 2012, pp. 57-62.

K.-T. Teng, and T.-C. Tsao, "A comparison of inversion based iterative learning control algorithms", submitted to American Control Conference, 2015

CHAPTER 1

Introduction

According to International Energy Agency, global electricity demand increases every year from 117,687 TWh in 2000 to 143,851 TWh in 2008 [Age12]. As the energy consumption keeps climbing, concerns about transmission costs, power quality, and the lack of power generations for localized demand are crucial for the future power distribution system. Researchers strives to find alternatives to typical radial form power distribution systems, the deployment of distributed generation(DG) across the grid seems to be a logical and reasonable solution to the aforementioned issues. Those DGs are usually small in size and adapt to local resources, they utilize renewable energy and provide an alternative way to traditional centralized power system [CN09].

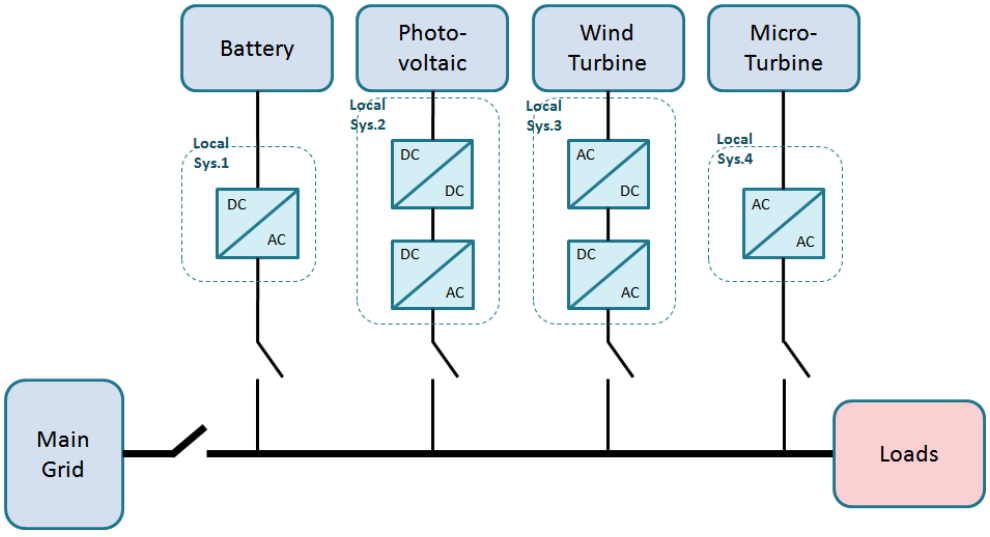

Figure 1.1: Schematic of a Micro-grid system

In order to convert the energy to compatible AC power in the grid, a power electronic system is required for most of the DG. Depending on the type of DG, the power electronic system may include inverter or rectifier or even both, as shown in Figure 1.1. All of the above DGs have to have power converters to be the interface between DG and main grid, either to drain current in phase with the voltage to obtain good power quality or to output compatible current into main grid [RBB07, KPB05, CMS02].

In addition to the microgrid system application, the power converters are also widely employed in uninterrupted power supply [RBL97], active power filter [CGF04, SMS03], PWM inverter motor drive [BK04, HNA10] and other industry facilities. Total harmonic distortion (THD) is one important index to evaluate the performance of the power converters. The harmonics lead to core loss in motors, malfunctions in solid state devices, excessive heating, etc.

The typical controller design for power converters is to have a high bandwidth inner current control loop with a low bandwidth outer voltage control loop [ZH03]. The controller design for DC power converters to have zero steady state error is pretty easy, since both voltage and current are constant in steady state. However, it is challenging to design a controller without steady state error for AC power converters, due to their variant voltage and current. In the literature, a DQ transformation is proposed to convert the AC variables into DC quantities. After the transformation, a well-designed Proportional-Integral controller can reduce the errors of the fundamental component to zero in steady state [RBB07, ZCS02, SAG04].

Although PI control in DQ rotating frame guarantee zero steady state error, it does not compensate for the harmonics other than fundamental. In order to have compensation for other harmonics, a repetitive control, based on internal model principle [FW76], is proposed and applied to the power converters to compensate for harmonics. However, the power rectifier is a non-linear system, the

input variable is coupled with the AC current. In order to linearize the model, the equilibrium points have to be chosen. In [SSP03], the equilibrium point of the AC quantities are chosen to be the RMS value. However, the operation point of AC voltage ranges from V_{peak} to $-V_{peak}$. In this thesis, we propose to linearize the system in the DQ rotating frame where all the AC quantities become DC variables. It makes the chosen of equilibrium points more meaningful. While applying DQ transformation doubles the system states and it also adds coupling effect between states. Therefore, a repetitive control for multi-input multi-output system is proposed to control the power converters in DQ rotating frame to compensate for harmonics.

Aside from learning control algorithms for power converters, the model-based iterative learning control for precision motion control is also proposed in this research. Iterative learning control (ILC) is a commonly used control methodology for applications that execute the same task multiple times [BTA06, ACM07, CMY06, KT04, SO91]. For these systems, the tracking reference has the same length and keeps unchanged from one run to the next. This feature implies that the error signal from the previous run has rich information. The objective of ILC is to minimize the tracking error by taking advantage of the error information from the previous runs to anticipate the control signal that can provide high-performance tracking result. In various industrial applications that execute repeated operation, ILC has shown its effectiveness on improving the performance. This includes industrial robots [Tay04, GN01, Ari90], computer numerical control machine [KT04], wafer stage motion systems [DB00, KK96, BA08], and chemical processing [CQL04].

The learning filter in ILC determines the performance of the algorithm, it decides how the past information will be used and which part of the information will be learned. The proportional type (P-type) and proportional-derivative type (PD-type) ILC are very popular among other learning filters [CL96, Saa94, CM02,

Ari90], since they do not require much knowledge about the system. However the tuning process for these two learning filters could be tedious and the learning process has to be reset whenever the parameters are adjusted. On the other hand, there are several popular model-based ILC algorithms such as model inversion methods, H_∞ methods, and quadratically optimal design methods [BTA06]. Model inversion methods use the inverse of the system dynamic as the learning function. H_∞ methods formulate the problem into linear fractional transformation form and solves the model mismatch problem. In quadratically optimal design methods, the learning function is defined in the lifted domain that minimizes the quadratic cost criterion for the next iteration where the estimation is based on the knowledge of the system model. The above model-based algorithms utilize the system model in different manner but the performance is mainly determined by the closeness of the model to the actual system.

For all different types of ILC algorithm, the idea behind designing or tuning the learning function is to approximate the inverse of the system dynamic so that the control law can be updated towards the optimal control for a given reference. In the case of P-type and PD-type ILC, the approximation is made by tuning proportional and derivative gains which constitutes a first order learning filter. A first order filter may be able to capture the trend of the system dynamic while high order dynamics could be missing which limits the convergence rate and the steady state error for P-type and PD-type ILC.

In model-based ILC algorithms, learning function is obtained from the knowledge of system dynamics. Although different algorithm formulates the learning function differently, the main idea is to find a learning filter that is closest to the inverse of the system dynamics. For model inversion based ILC, the learning function is simply chosen to be the inverse of the system dynamics. If the system dynamic is invertible, the tracking error should converge to zero within one iteration. While the system has non-minimum phase zero, the inversion of the system will

become an unstable filter. In the literature, there are several methods that approximate the inversion of non-minimum phase system. In time domain, zero-phase-error tracking controller (ZPETC) [Tom87, TT87, KT14b], zero-magnitude-error tracking controller (ZMETC) [RPL09], and direct inversion [CT14, CT13] have been used to invert non-minimum phase system. In frequency domain, Model-less Inversion-Based Iterative Control (MIIC) [KZ08] has been applied to inverse the dynamic of atomic force microscope.

In this thesis, a data-based dynamic inversion method in frequency domain is proposed to approximate the inverse of system dynamic. It utilizes the information from testing data in frequency domain to construct the learning function which not only reduces the unmodeled dynamics but also gets around the issue of inverting non-minimum phase system. All the aforementioned inversion methods are implemented on a linear motor for tracking a non-circular piston profile and a 50 Hz triangle wave. The performance is compared in terms of convergence rate and final converged error.

The remainder of the thesis is organized as follows: In Chapter 2, the Repetitive control for MIMO system will be introduced. Smith-McMillan decomposition method is used to decoupled the MIMO system to enable the design of prototype repetitive control. And then the proposed MIMO repetitive control is implemented to control the power inverter and power rectifier in Chapter 3 and 4 respectively. In Chapter 5, the design of model-based iterative learning control is presented. Finally, the concluding remarks are made in Chapter 6.

CHAPTER 2

Repetitive Control for Multi-Input Multi-Output (MIMO) System

In [TTC89], the prototype repetitive control design for single-input single-output system is presented. The analysis shows that in order to satisfy the stability condition, the designed repetitive controller has to satisfy the Diophantine equation. One of the solution to that is the Zero-Phase-Error-Tracking-Controller (ZPETC).

In this chapter, the Smith-McMillan decomposition method is used to transform the original coupled MIMO system into a coordinate where the states are decoupled. Within the transformed coordinate, the ZPETC design can be implemented on the diagonal SISO system. Therefore, the prototype repetitive control can be applied to the SISO system in the transformed coordinate directly.

2.1 Prototype Repetitive Control

Consider the feedback control system shown in Figure 2.1, where P is the open loop plant model, C is the stabilizing feedback controller, and d is the disturbance signal composed of multiple harmonics of know frequency ω. And the closed-loop system can be defined as

$$G = \frac{CP}{1+CP} = z^{-d}\frac{B}{A} \tag{2.1}$$

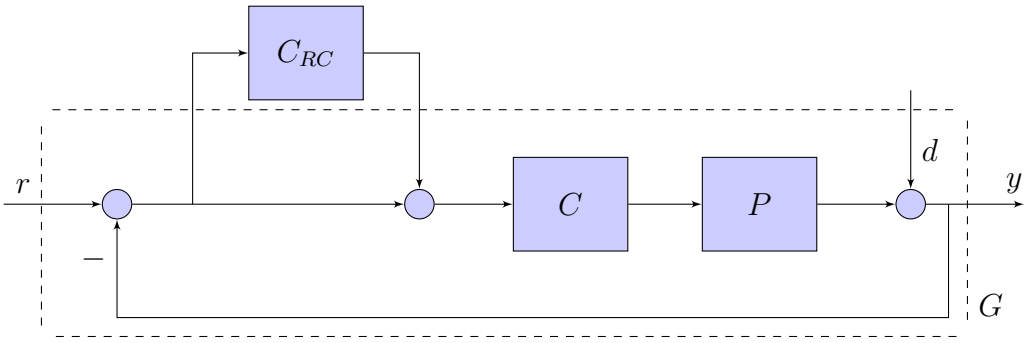

Figure 2.1: The repetitive control C_{RC} is plug-in to an existing stable feedback loop

According to internal model principle [FW76], in order the reject the sinusoidal disturbance, the feedback loop has to incorporate the disturbance model. The internal model is implemented by using a positive feedback loop wrapped around a group delay that corresponds to the period of the sinusoidal signal. A general from of the repetitive controller can be described by

$$C_{RC} = \frac{1}{1 - z^{-N}} \cdot \frac{R}{S} \tag{2.2}$$

In [TTC89], it shows that the class of (S, R) that guarantees asymptotically stability corresponds to solve a high order Diophantine equation. But a special case under this class of stabilizing controller is proposed

$$\frac{R}{S} = k_r \frac{z^{-N+d} A B^{-*}}{B^{+}} \tag{2.3}$$

which is the ZPETC for the preexisting stable closed loop system.

Although the above prototype repetitive control design is mainly for SISO systems, the major hinder for applying it MIMO system is the formulation of ZPETC. If one can find a ZPETC for the MIMO stable closed loop system $\mathbf{G}$ such that

$$\mathbf{FG} = \begin{bmatrix} d_1 & & & \\ & d_2 & & \\ & & \ddots & \\ & & & d_n \end{bmatrix} \tag{2.4}$$

where d_i are linear phase filters. Then the prototype repetitive control design can be applied to every diagonal filters individually.

2.2 Multi-variable Zero-Phase-Error-Tracking-Control

In this section the Zero-Phase-Error-Tracking-Control algorithm for MIMO system is presented. The ZPETC is first introduced in [Tom87] for SISO plant, the concept is to cancel the phase distortion from the unstable zeros by including the complex conjugate of the unstable zeros in the inversion filter. In [Tsa88], Tsao proposed the idea of extending the ZPETC to MIMO plant can be implemented by utilizing Smith-McMillan decomposition [Mac89]. But no applications of using ZPETC to MIMO system for designing repetitive control has been published.

This section will present the design of ZPETC for MIMO system that enables the prototype repetitive control to MIMO systems.

2.2.1 Smith-McMillan Form

The Smith-McMillan form is used to factorize the poles and zeros of a transfer function matrix with multiple inputs and outputs.

Definition 1. *A matrix* $\boldsymbol{P}^{n\times m} = [p_{ij}(z)]$ *is a* ***polynomial matrix*** *if* $p_{ij}(z)$ *is a polynomial in* z *for* $i = 1, 2, \ldots n$ *and* $j = 1, 2, \ldots m$.

Definition 2. *A* ***unimodular matrix*** *is a polynomial matrix that its determinant is a constant.*

Definition 3. *The **elementary operation** of a polynomial matrix is the same as of a real matrix, and it is one of the following:*

- *Interchange of two rows of columns*
- *multiplication of one row or column by a constant*
- *addition of one row/column to another row/column times a polynomial*

Definition 4. *Two polynomial matrices $\boldsymbol{P}(z)$ and $\boldsymbol{D}(z)$ are **equivalent**, if there exists a set of elementary matrices $\boldsymbol{L}_i$ and $\boldsymbol{R}_i$ such that*

$$\boldsymbol{D}(z) = \boldsymbol{L}_1(z)\boldsymbol{L}_2(z)\cdots\boldsymbol{L}_{n1}(z)\boldsymbol{P}(z)\boldsymbol{R}_1(z)\boldsymbol{R}_2(z)\cdots\boldsymbol{R}_{n2}(z) \tag{2.5}$$

Using the aforementioned notation, if we choose the suitable set of $\mathbf{L}_i$ and $\mathbf{R}_i$ matrices, the original polynomial matrix $\mathbf{P}^{n\times m}$ can be transformed into a pseudo-diagonal $n \times m$ matrix $\mathbf{D}(z)$, the Smith form:

$$\mathbf{D}(z) = diag(d_1(z),\ d_2(z), \cdots,\ d_r(z),\ 0, \cdots,\ 0) \tag{2.6}$$

where r is the rank of $\mathbf{P}(z)$ and $d_i(z)$ is a factor in $d_{i+1}(z)$.

Suppose $\mathbf{G(z)}^{n\times m}$ is a $n \times m$ transfer function matrix, where n is the number of outputs and m is the number of inputs, and the rank of $\mathbf{G(z)}$ is r. We will write the transfer function matrix in the following form,

$$\mathbf{G}(z) = \frac{1}{A(z)} \cdot \mathbf{P}(z) \tag{2.7}$$

Just as the polynomial matrix $\mathbf{P}(z)$ can be transformed into a pseudo-diagonal matrix $\mathbf{D}(z)$, the transfer function matrix $\mathbf{G}(z)$ is equivalent to a pseudo-diagonal transfer function matrix. This matrix $\mathbf{M}(z)$ is the Smith-McMillan form of the transfer matrix $\mathbf{G}(z)$.

Theorem 1. ***(Smith-McMillan from).*** *Let* $\boldsymbol{G(z)} = [G_{ij}(z)]$ *be an* $m \times m$ *transfer function matrix,*

$$\boldsymbol{G}(z) = \frac{\boldsymbol{P}(z)}{A(z)} \tag{2.8}$$

where $\boldsymbol{P}(z)$ *is an* $m \times m$ *polynomial matrix of rank* r *and* $A(z)$ *is the least common multiple of the denominators of all elements of* $G_{ij}(z)$*. Then* $\boldsymbol{G}(z)$ *can be transformed to a pseudo-diagonal transfer function matrix* $\boldsymbol{M}(z)$ *by proper choice of* $\boldsymbol{L}(z)$ *and* $\boldsymbol{R}(z)$ *as*

$$\boldsymbol{M}(z) = L(z)\,\boldsymbol{G}(z)R(z) \tag{2.9}$$

$$= diag[\frac{m_1(z)}{a_1(z)},\ \frac{m_2(z)}{a_2(z)}, \cdots,\ \frac{m_r(z)}{a_r(z)},\ 0, \cdots,\ 0] \tag{2.10}$$

where $\frac{d_i(z)}{A(z)} = \frac{m_i(z)}{a_i(z)}$ *after all the possible cancellations being performed.*

2.2.2 ZPETC for MIMO plant

For a given MIMO plant $\mathbf{G}^{m\times m}(z)$, let $\mathbf{F}(z)$ be

$$\mathbf{F}(z) = \mathbf{R}(z)\mathbf{N}(z)\mathbf{L}(z) \tag{2.11}$$

where

$$\mathbf{N}(z) = diag\left[z^{-nu}\frac{a_i(z)m_r^-(z)(m_{ri}^-(z))^*}{bm_i^+(z)}\right] \tag{2.12}$$

where $m_{ri}^-(z)$ represents the unstable zeros that are in $m_r(z)$ but not in $m_i(z)$, and nu is the number of unstable zeros in $\frac{m_r(z)}{a_r(z)}$.

The transfer function of $\mathbf{FG}$ can be written as

$$\mathbf{FG} = \mathbf{R}(z)\mathbf{N}(z)\mathbf{L}(z)\mathbf{L}^{-1}(z)\mathbf{M}(z)\mathbf{R}^{-1}(z) \tag{2.13}$$

$$= \mathbf{R}(z)diag\left[z^{-nu}\frac{a_i(z)m_r^-(z)(m_{ri}^-(z))^*}{bm_i^+(z)}\right] diag\left[\frac{m_1(z)}{a_1(z)},\ \frac{m_2(z)}{a_2(z)}, \cdots,\ \frac{m_r(z)}{a_r(z)}\right]\mathbf{R}^{-1}(z) \tag{2.14}$$

$$= z^{-nu}\frac{m_r^-(z)(m_r^-(z))^*}{b}\cdot\mathbf{I} \tag{2.15}$$

where b is a scalar to compensate for the magnitude of $\mathbf{FG}$.

Although this section only shows the extension of SISO ZPETC to MIMO plant, other dynamic inversion method for SISO plant can be applied as well.

For Zero-Magnitude-Error-Tracking-Control [RPL09], the diagonal transfer function matrix $\mathbf{N}(z)$ will be,

$$\mathbf{N}_{zm}(z) = diag\left[\frac{a_i(z)m_{ri}^{-}(z)}{m_i^{+}(z)(m_r^{-}(z))^*}\right] \tag{2.16}$$

where $m_{ri}^{-}(z)$ represents the unstable zeros that are in $m_r(z)$ but not in $m_i(z)$.

For Direct Inversion [CT14],

$$\mathbf{N}_{di}(z) = diag\left[\left(z^{-nu}\frac{a_i(z)}{m_i(z)}\right)_{FIR}\right] \tag{2.17}$$

where nu is the length of the FIR filter being used to approximate the dynamics of the unstable zeros.

CHAPTER 3

Repetitive Control of Power Inverter for Harmonic Compensation

In this chapter, the Voltage Source Inverter (VSI) will be introduced. The Sinusoidal-Pulse-Width-Modulation technique is used to drive the Insulated-gate bipolar transistor (IGBT) switches on the inverter. Sampling process is synchronized with the PWM carrier signal to reconstruct the average signal value while violating Nyquist sampling theorem. A Proportional-Integral control is first used in fixed frame to provide baseline performance. Since PI can only guarantee zero steady sate error for constant reference/disturbance, the tracking error is expected to be significant. In [ZCS02] a D-Q rotating transformation technique is proposed for single phase power inverter into convert AC variables to DC quantities. Therefore, PI control in D-Q rotating frame will have zero steady state error at fundamental frequency. However harmonics other than fundamental are not being taken care of.

In order to tack given AC voltage waveform and compensate for its harmonics, repetitive control is further introduced to both fixed frame and rotating frame. The repetitive control design is straightforward in fixed frame where the prototype repeititve control [TTC89] can be applied directly. However, in rotating frame, the original Single-Input Single-Output (SISO) system becomes Mulit-Input and Multi-Output (MIMO) system coupled by the frequency of the AC variables which makes the repetitive control design challenging. The Repetitive control for Mulit-Input and Multi-Output system introduced in Chapter 2 will be applied to design

the repetitive control in D-Q rotating frame for power inverter.

Different control methods are implemented to the power inverter. The experimental results will be presented to compare the performance of tracking error and total harmonic distortion (THD) of the output voltage.

3.1 Introduction of Power Inverter

Figure 3.1 shows the typical topology of single phase full bridge voltage source inverter (VSI). The VSI plays a vital role in microgrid applications, it converts power from different power generations into AC power that is compatible with grid power. There are two modes of operation for VSI in microgrid application: Grid-tied and Off-grid. When the VSI is connected to the grid, the control objective is to output maximum current while maintain the phase of the output current in phase with the grid voltage; In off-grid mode, the control object is to maintain the output voltage at desired magnitude and frequency.

The output AC voltage can be controlled by switching the full-bridge in an appropriate manner. The Sinusoidal-PWM scheme is used to generate the proper gating signals for the switches in full-bridge inverter to control the amplitude and frequency of the output AC voltage. In order to have a clean AC power output, a control method that can compensate for harmonics is required.

The total harmonic distortion (THD) of a signal is a measurement of the harmonic distortion present and is defined as the ratio of the sum of the powers of all harmonic components to the power of the fundamental frequency, as shown in Equation 3.1. In electrical power systems, lower THD means reduction in peak currents, heating, emissions, and core loss in motors.

$$THD = \frac{\sqrt{V_2^2 + V_3^2 + \cdots + V_n^2}}{V_1} \tag{3.1}$$

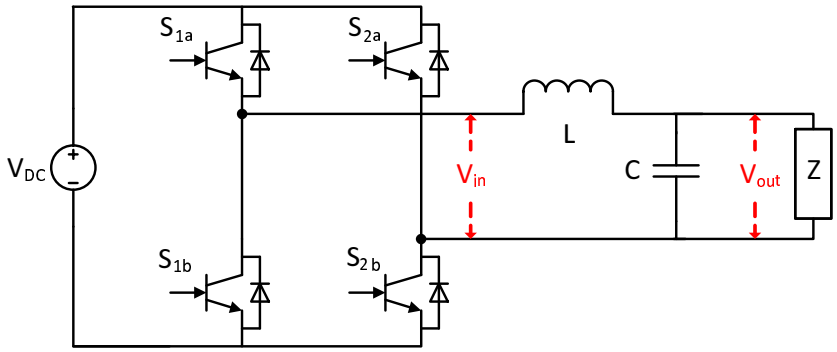

Figure 3.1: Circuit schematic of Singel-Phase Full Bridge PWM Invereter: the objective is to have the output voltage V_{out} in phase with given AC voltage waveform with small total harmonic distortion (THD)

3.2 System Configuration

The switching function of the upper and lower transistor in arm n as shown in Figure 3.1 are represented by s_{na} and s_{nb} respectively. When switch is closed, it corresponds to $s_x = 1$. And the condition $s_x = 0$ imply open switch. And the following switching constraint is imposed to avoid short circuit on the DC source,

$$S_{na} + S_{nb} = 1 \tag{3.2}$$

Using the switching function defined in 3.2, the input voltage to the LC filter, V_{in}, can be related to the DC link voltage, V_{DC} as,

$$V_{in} = (S_{1a} - S_{2a})\, V_{DC} \tag{3.3}$$

The derivative of the inductor current can be written as,

$$L\frac{dI_L}{dt} = V_{in} - V_{out} \tag{3.4}$$

The derivative of the capacitor voltage can be represented as,

$$C\frac{dV_c}{dt} = I_L - \frac{1}{Z}V_{out} \tag{3.5}$$

Combining Equation 3.3-3.5, the following state-space model can be obtained,

$$\frac{d}{dt}\begin{bmatrix} I_L \\ V_{out} \end{bmatrix} = \begin{bmatrix} 0 & -\frac{1}{L} \\ \frac{1}{C} & -\frac{1}{ZC} \end{bmatrix} \cdot \begin{bmatrix} I_L \\ V_{out} \end{bmatrix} + \begin{bmatrix} \frac{1}{L} \\ 0 \end{bmatrix} \cdot V_{in} \tag{3.6}$$

As the switching frequency of the PWM is very fast with respect to the dynamic of the electrical system, the converter may be modeled as continuous system by applying the average operator

$$\bar{x}(t) = \frac{1}{T}\int_{t-T}^{t} x(\tau)d\tau \tag{3.7}$$

where T is the period of the PWM carrier signal.

3.2.1 Sinusoidal-Pulse-Width-Modulation

As mentioned in Equation 3.2, the switching constraint is added to the PWM modulation so that the short circuit on the DC source can be avoided. Figure 3.2 shows the generation of gating pulses for driving the full-bridge switches shown in Figure 3.1.

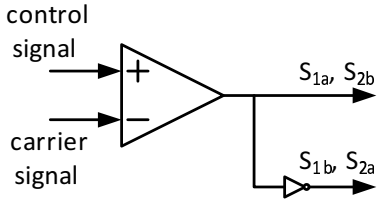

Figure 3.2: The gating pulses is generated by comparing the control signal with the carrier signal.

Figure 3.3 shows an example of a SPWM process while the control signal is a sinusoidal signal. The third plot is the output from the comparator, and the

fourth plot is the complement of that. From Equation 3.3, the input voltage to the LC filter can be constructed by using the gating pulses from third and fourth plot, and the result is shown as the blue line in the bottom plot. It is evident that while the output of the comparator changes, all four switches are going to change states at the same time. Due to the commutation time requires for non-ideal switches, a proper dead-time is necessary for driving the full-bridge switches. In other words, a short period of delay has to be added before the switch-on gating signal is being sent to the gate. Otherwise, this would result into a short circuit across the input DC source voltage, leading to current circulation through the full-bridge.

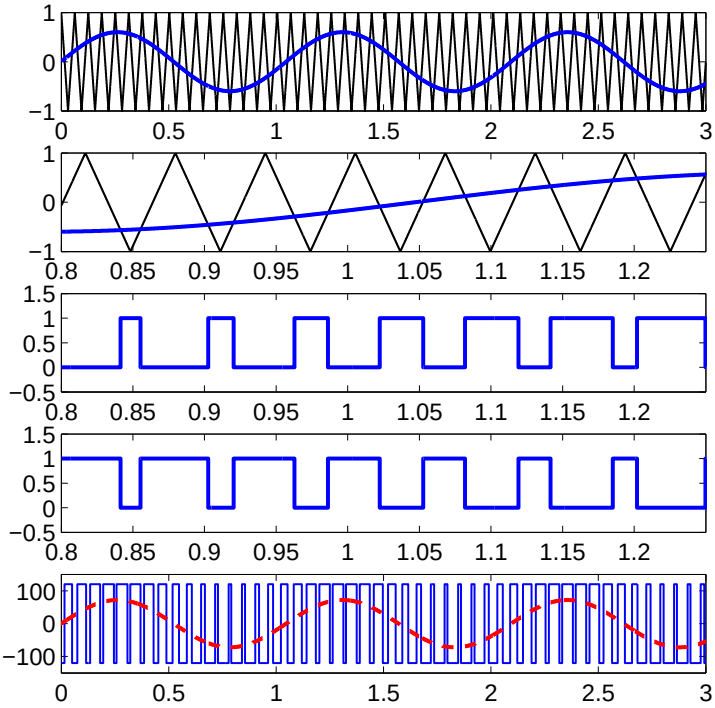

Figure 3.3: Example of a SPWM process: the control signal (blue in top two plots) is compared with the carrier signal (black in top two plots), and the gating pulses are generated (in third and fourth plots). After filtering V_{in} through the low-pass LC-filter, the sinusoidal output voltage, V_{out}, can be expected.

In the experiment, both of the comparator circuit and the dead-time are being implemented on the Field-programmable gate array (FPGA) in a 40 Mhz loop. The IGBT switches used in this thesis has turn-on time at 420 ns, for extra safety the dead-time is chosen to be 1 μs

3.2.2 Synchronization of Sampling and PWM

As stated in Section 3.2, the power inverter is controlled by the PWM modulator which will create high frequency ripples on the output power. According to Nyquist sampling theorem, the sampling rate should be at a frequency that the spectrum of the signal is negligible at the Nyquist frequency. This would require a sampling frequency at least a order of magnitude higher than the switching frequency. But the hardware capability limits the sampling frequency from being too fast, the Nyquist sampling theorem has to be violated.

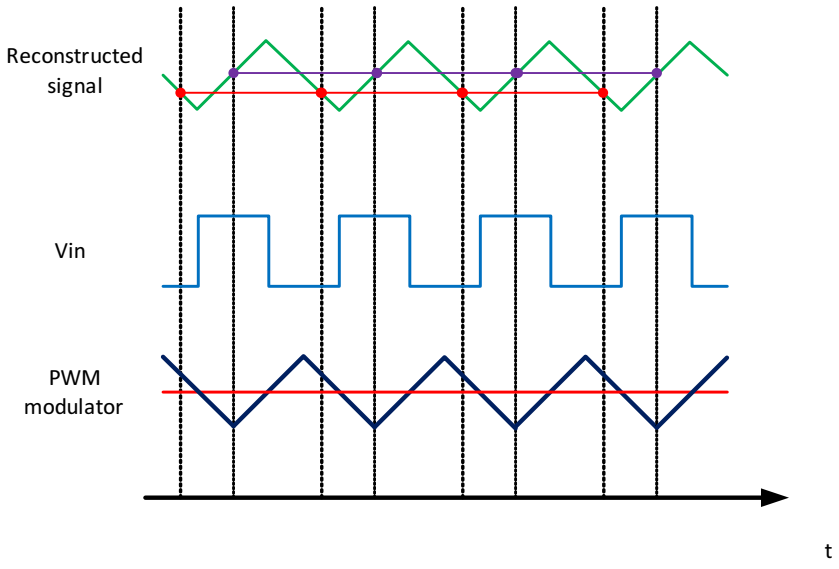

Figure 3.4: Example shows the effect of sampling timing: If the sampling is synchronized with PWM, the averaged signal can be reconstructed (purple line). While the sampling is not properly synchronized with PWM, the sampled data may be off from the average signal (red line)

However, if the sampling processes are synchronized with the PWM carrier signal properly, the effect of aliasing can be attenuated and the sampled data will be in close proximity to the average value of the actual signal. This effect can be observed from Figure 3.4, the reconstructed signal will be the average value of the actual signal if the sampling process takes place in the middle of the on or off state of the gating pulses. And the on/off state of the gating signal is either the beginning of the end of each period of the PWM carrier signal. In other words, the fastest sampling frequency without aliasing effect can only be as fast as twice the switching frequency. When the sampling rate is slower than the switching frequency, the sampling frequency has to be chosen such that the switching frequency is an integer multiple of the sampling frequency.

3.2.3 Real-Time Control System

In the power inverter system shown in Figure 3.1, signals that are being measured are the input DC voltage, V_{DC}, output AC voltage, V_{out}, and the inductor current, I_L. Both of the voltage sensors are simple voltage divider that step down the voltage to the range of the digital input port; a hall effect sensor with gain 1 mA/mV is used for current sensing.

Unlike the conventional double loop control structure with inner current loop and outer voltage loop, this research only uses the voltage controller to close the loop. And the control signals are the gating pulses that generated from the PWM driver.

National Instruments Reconfigurable IO card NI-7833R process both sensor and control signals, as shown in Figure 3.5. The Field Programmable Gate Array (FPGA) is used to sample the analog signals and generate the gating signals for the switches. All the low level control ans sensing utilities are being executed in the FPGA, including PWM modulator, synchronization between sampling and

PWM, and the dead time delay. A personal computer serves as the real-time processor that executes the control algorithm and communicate with the FPGA. The control software is coded using National Instruments LabVIEW, LabVIEW FPGA module, and LabVIEW RealTime module.

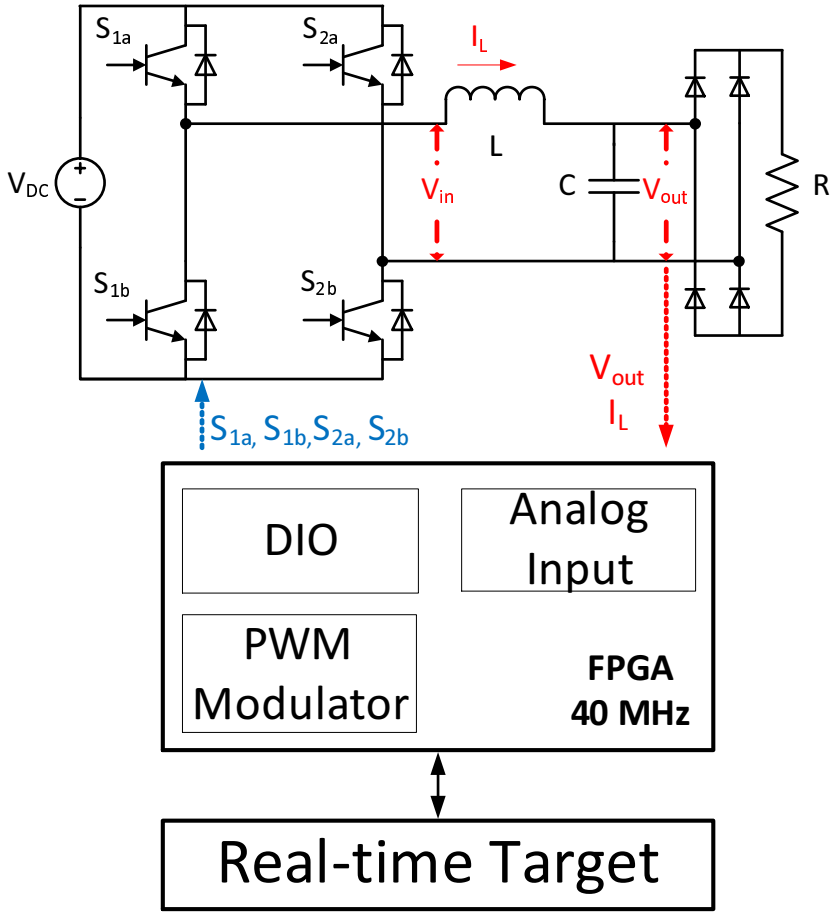

Figure 3.5: Block diagram of LabVIEW real-time control system

3.3 AC Voltage Tracking with PI Control

In this section, the Proportional-Integral controller is designed to control the power inverter to track the 60 Hz sinusoidal AC voltage with small harmonics. Figure 3.6 shows the spectrum of output voltage while the power inverter is operating without any control action. The spectrum of the output voltage contains components at

odd harmonics up to 27th order. The control objective is to track the given 60 Hz sinusoidal AC voltage while compensate for the harmonics.

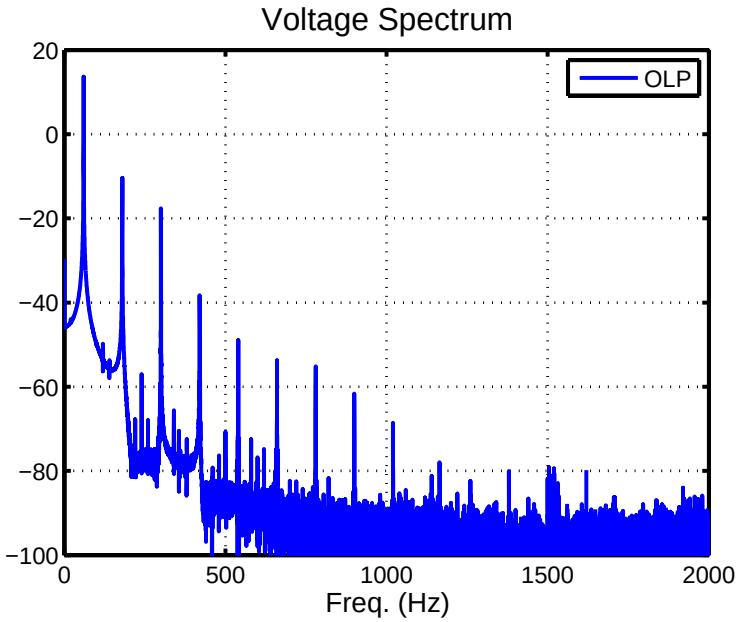

Figure 3.6: Spectrum of output voltage for open loop system (THD = 7.096 %)

3.3.1 Modeling of power inverter

Although the continuous time model of the power inverter can be derived by applying the average operator to Equation 3.6, the actual experimental kit is an out-of-shelf product which has extra components damping out the resonant from the analytical model.

3.3.1.1 Fixed frame

Using a psuedo-random binary signal (PRBS) excitation on a open-loop system, a time domain system identification is performed with MATLAB System Identification Toolbox. Using N4SID model fitting, a second order open-loop system is identified as shown in Figrue 3.7.

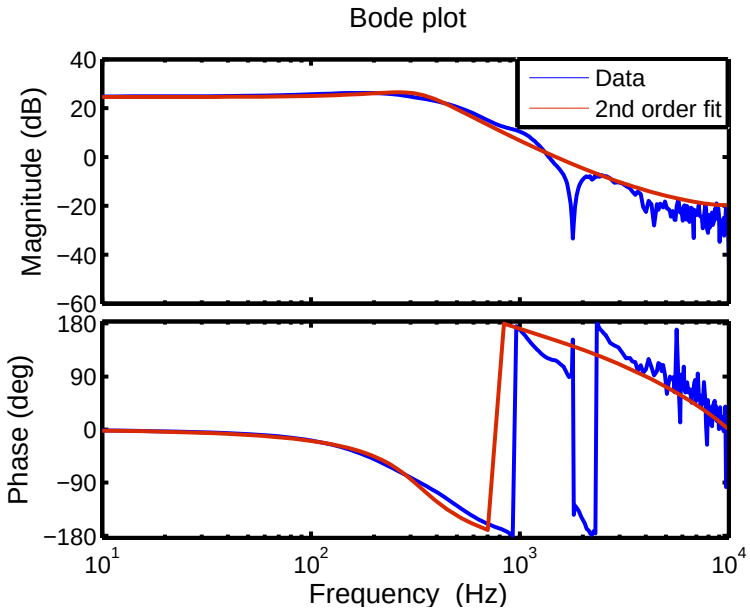

Figure 3.7: Curve fit of open loop system

3.3.1.2 Rotating frame

One of the control objective of power inverter is maintaining the output voltage at desired magnitude and phase. Those quantities are sinusoidal waveforms in fixed frame but DC values in DQ rotating frame. By transforming the averaged model into DQ rotating frame, a properly designed PI controller can guarantee zero steady state error on the output current or voltage.

However, the transformation from stationary frame to DQ rotating frame requires two orthogonal quantities. In three phase power systems, the original components within ABC frame are first being transformed to the stationary $\alpha\beta$ frame where all the quantities are in pair and orthogonal. Then the DQ transformation matrix in (3.8) is applied to further transform the orthogonal components into synchronous DQ rotating frame.

$$\begin{bmatrix} v_d \\ v_q \end{bmatrix} = \begin{bmatrix} \cos\theta & \sin\theta \\ -\sin\theta & \cos\theta \end{bmatrix} \cdot \begin{bmatrix} v_\alpha \\ v_\beta \end{bmatrix} \tag{3.8}$$

In single phase power systems, the AC components do not appear in pairs which does not satisfy the criteria for applying DQ transformation. However, we can construct a fictitious circuit that is in parallel with the real circuit, as shown in Figure 3.8. Assuming all the components in the two circuits are identical expect that the control command to the fictitious circuit has a 90^o phase lag than the real circuit, then all the variables in the two circuit will be orthogonal components [ZCS02].

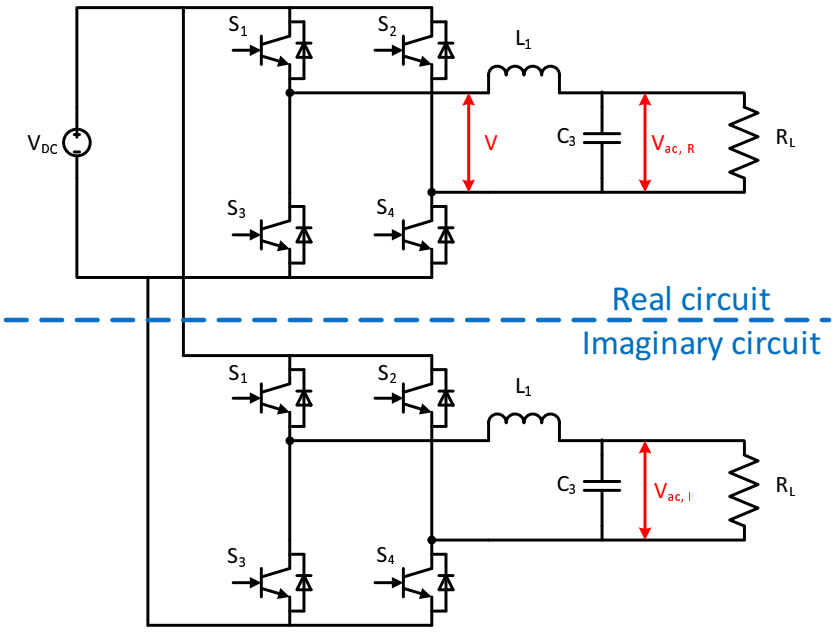

Figure 3.8: The variables from the fictitious circuit enables the DQ transformation for single-phase circuit.

Applying the DQ transformation matrix in Equation 3.8 to the fixed frame model in Equation 3.6, the state-space model in the DQ rotating frame can be obtained,

$$\frac{d}{dt}\begin{bmatrix} I_d \\ I_q \\ V_d \\ V_q \end{bmatrix} = \begin{bmatrix} 0 & \omega & -\frac{1}{L} & 0 \\ -\omega & 0 & 0 & -\frac{1}{L} \\ \frac{1}{C} & 0 & -\frac{1}{Z_{load}C} & \omega \\ 0 & \frac{1}{C} & -\omega & -\frac{1}{Z_{load}C} \end{bmatrix} + \begin{bmatrix} \frac{V_{DC}}{L} & 0 \\ 0 & \frac{V_{DC}}{L} \\ 0 & 0 \\ 0 & 0 \end{bmatrix} \cdot \begin{bmatrix} D_d \\ D_q \end{bmatrix} \tag{3.9}$$

In the DQ rotating frame, the system becomes a multi-input multi-output system that coupled by the AC frequency ω. By applying the transformation matrix to the identified model in Figure 3.7, the frequency response in DQ rotating frame can be obtained in Figure 3.9.

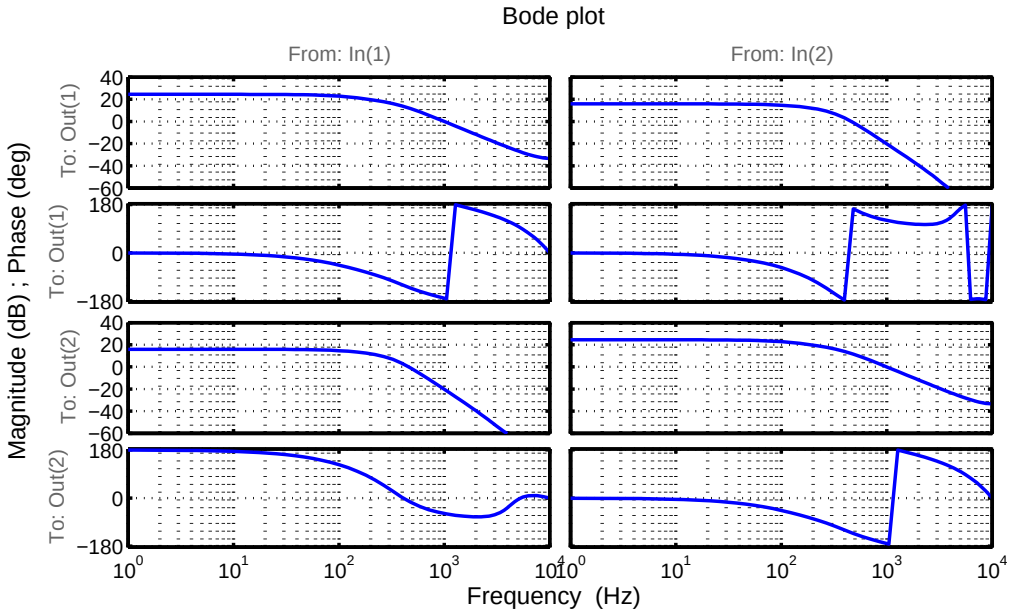

Figure 3.9: Curve fit of inverter model data in DQ frame

3.3.2 PI control in Fixed Frame

As the typical inverter control, a non-model based PI control for the power inverter is designed to guarantee zero steady state error. Since the tracking reference for power inverter is the output AC voltage, the PI control is not expected to do well.

Figure 3.10 shows the spectrum of the tracking error, it is evident that PI

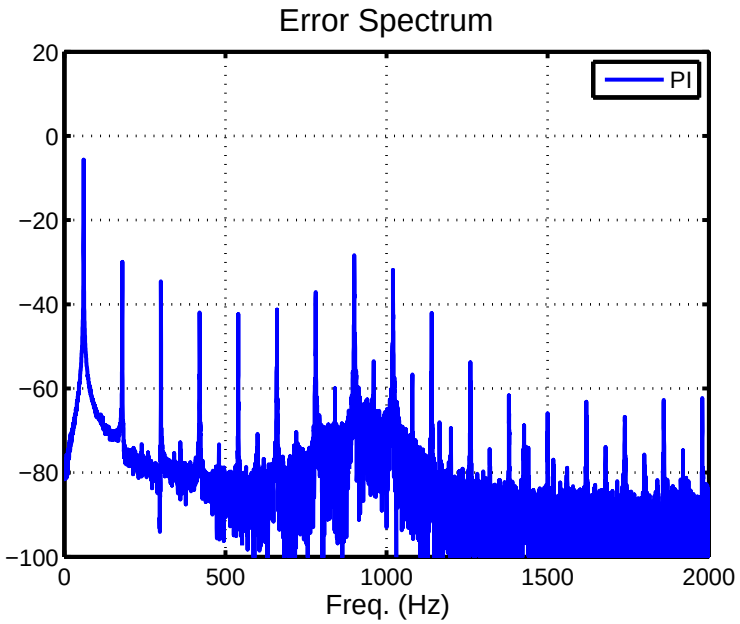

Figure 3.10: Spectrum of the tracking error on output voltage V_{out}

control is not able to track the sinusoidal AC voltage with zero steady state error. The phase lag in the closed loop system causes a large error at 60 Hz. In addition, the harmonics are still significant in the output voltage. Although it does attenuate the 3rd and the 5th harmonics by about 20 dB, the THD only gets reduced by 0.2% which means the other harmonics are not being affected.

In order to track the 60 Hz AC voltage better, and also increase the bandwidth of the PI controller, a DQ transformation that converts the AC variables into DC quantities will be introduced in the next section. By designing the PI control in the rotating frame, the 60 Hz AC voltage becomes DC variable. Meaning the PI control in the rotating frame will be able to guarantee zero steady state tracking error at 60 Hz.

3.3.3 PI control in Rotating Frame

In this section, the same PI control used in the fixed frame is used for both channel of the MIMO system. Figure 3.12 shows the frequency response of the closed-loop

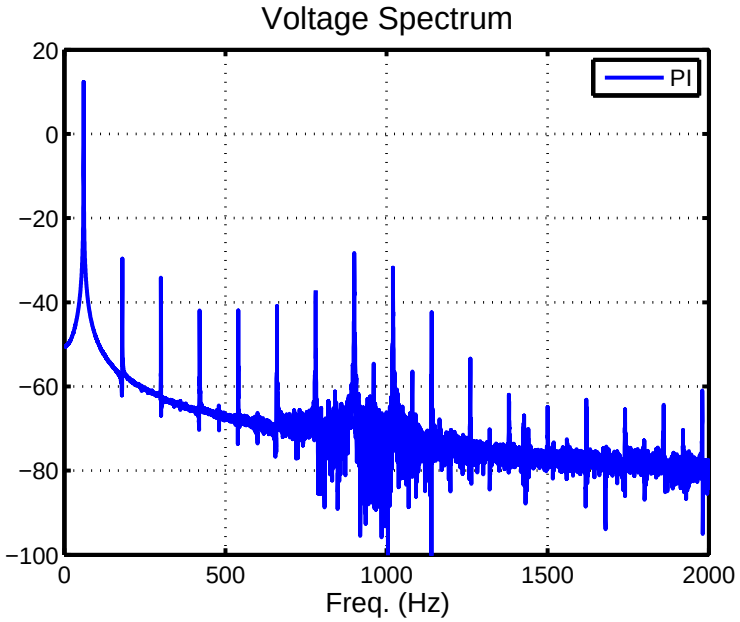

Figure 3.11: Spectrum of the output voltage V_{out}. (THD = 6.82 %)

MIMO system. Although the system is not fully decoupled by the PI control, the coupling effect at low frequency is pretty weak. The PI control is expected to have zero steady state error at 0 Hz which corresponds to 60 Hz in fixed frame.

The spectrum of the tracking error on output voltage, shown in Figure 3.13, validates that PI control in DQ rotating frame provides zero steady state tracking error as the magnitude of the spectrum at 60 Hz is below -60 dB. However, the other harmonics, especially odd harmonics, are not being taken care of by PI control. If we further look at the spectrum of the output voltage in Figure 3.14, the odd harmonics components are still significant.

The PI control has infinite loop gain at 0 Hz in DQ rotating coordinate which is 60 Hz in fixed coordinate. Therefore, a PI control in DQ rotating coordinate is actually an internal model principle (IMP) type controller. Meaning if we use an IMP type controller that can deal with multiple harmonics, the output voltage is expected to have better performance with smaller THD.

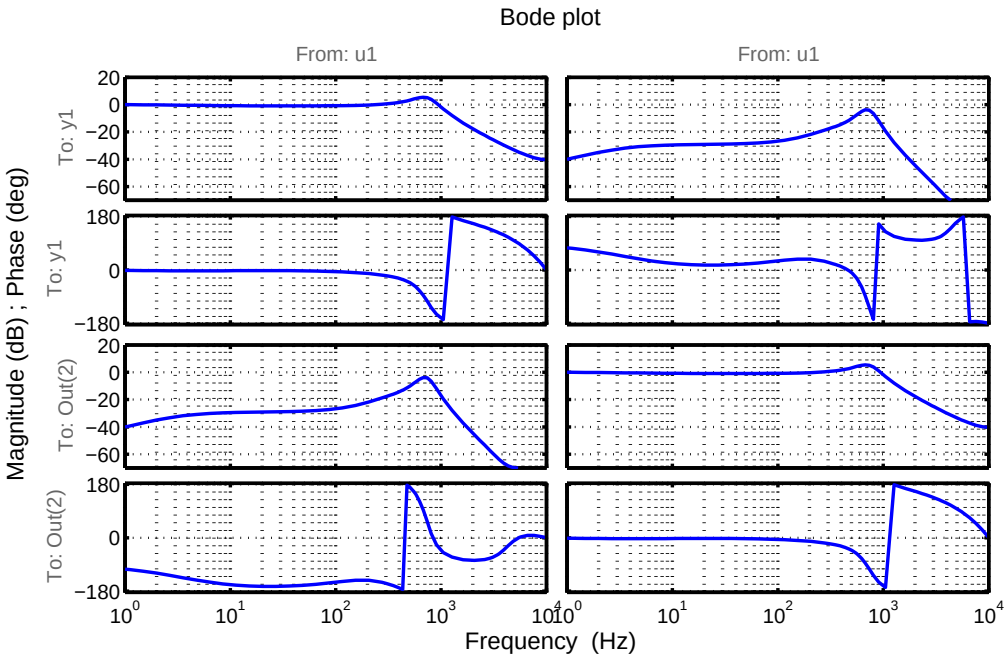

Figure 3.12: Frequency response of closed-loop system in DQ frame

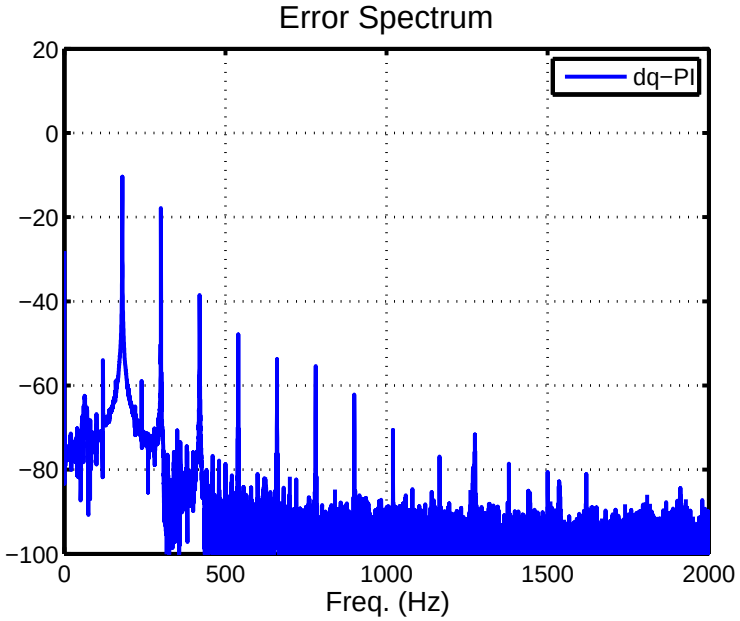

Figure 3.13: Spectrum of tracking error on output voltage V_{out}

3.4 Harmonic Compensation by Repetitive Control

In this section, the prototype repetitive control introduced in 2.1 will be used to control the power inverter. Since repetitive control uses a positive feedback

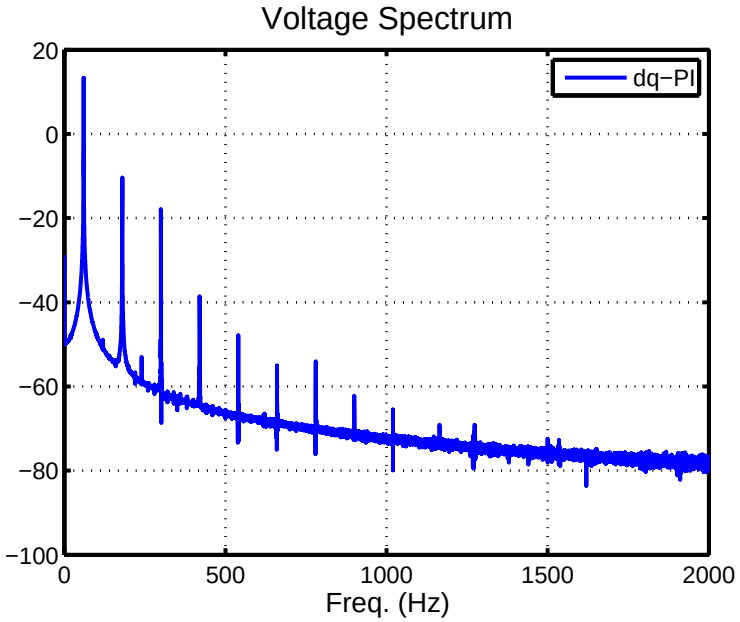

Figure 3.14: Spectrum of output voltage V_{out}. (THD = 2.5%)

loop wrapped around a group delay that corresponds to the period of 60 Hz sinusoidal AC voltage, it can not only provides perfect tracking but also rejects the disturbances at that frequency or its harmonics.

In 3.4.1, a plug-in repetitive control will be designed for the closed-loop system in the fixed frame. Since the power inverter is a single-input single-output in fixed frame, the prototype repetitive control [TTC89] can be applied directly. In section 3.4.2, we proposed to design the repetitive control in the DQ rotating coordinate where the power inverter becomes a MIMO system. The repetitive control for MIMO system design methodology introduced in 2 will be used.

3.4.1 Repetitive Control in Fixed Frame (SISO)

3.4.1.1 Prototype Repetitive Control

The identified model shown in Figure 3.7 is used to design the prototype repetitive controller in equation 2.2. In order to incorporate model uncertainty in the

control design, a Q-filter is added into the repetitive control structure as shown in Figure 3.15.

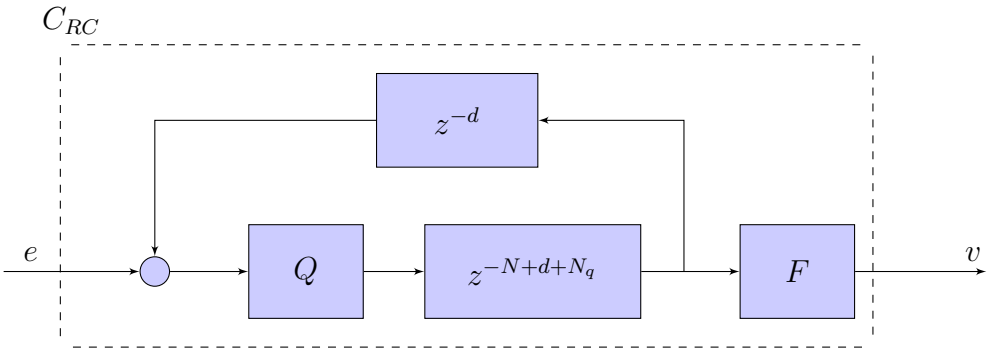

Figure 3.15: Block diagram of plug-in repetitive control

To ensure stability, repetitive control design must satisfy

$$\|(1 - FG)Q\| < 1 \tag{3.10}$$

where $\|\cdot\|$ is abuse of notation and the precise meaning is the magnitudes are smaller than 1 across all frequencies. And the Q-filter is typically chosen to be a linear phase low-pass filter for maintaining robust stability and the zero-phase property [TT94].

Assuming the actual system dynamic is represented by G_a, then the left hand side of the Equation 3.10 can be written as,

$$\|(1 - FG_a)Q\| = \|(1 - FG + FG - FG_a)Q\| \tag{3.11}$$

$$\approx \|(FG - FG_a)Q\|, \quad where\ |FG| \approx 1 \tag{3.12}$$

$$= \|FG\left(\frac{G - G_a}{G}\right)Q\| \tag{3.13}$$

$$\approx \|\frac{G - G_a}{G} \cdot Q\| \tag{3.14}$$

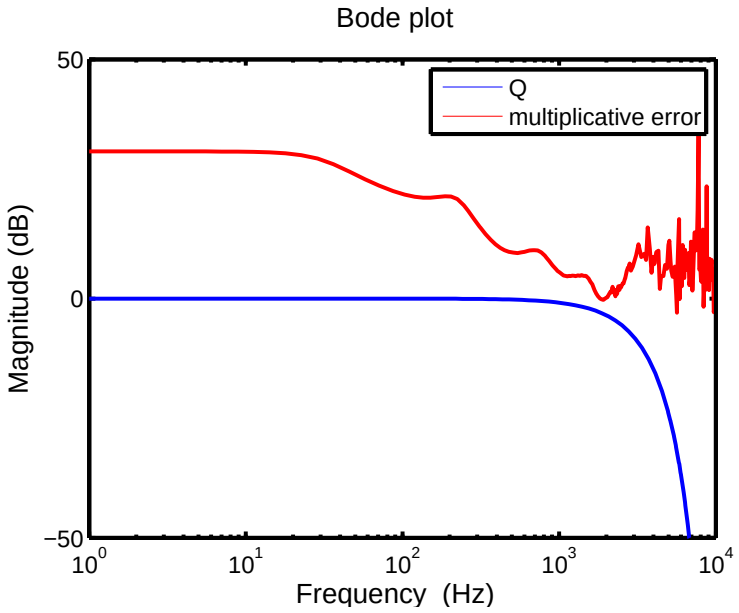

Figure 3.16: Magnitude of Q-filter and inverse of multiplicative modeling error for robust stability of power inverter

Combining Equation 3.10 and 3.14, a sufficient condition for robust stability is

$$\|Q\| < \|\frac{G}{G - G_a}\| \tag{3.15}$$

Figure 3.16 shows the magnitude of Q-filter and the inverse of multiplicative modeling error. The Q-filter is chosen to be

$$Q = \left(0.25 + 0.5z^{-1} + 0.25z^{-2}\right)^n \tag{3.16}$$

with $n = 4$

Figure 3.17 shows the spectrum of the tracking error, repetitive control not only tracks the 60 Hz AC voltage with error at -65.8 dB but also suppress all the harmonics below -50 dB. The output voltage spectrum in Figure 3.18 further shows that the highest component among all harmonics is at 3rd harmonic with magnitude at -50 dB, and the THD is being reduced to 0.14 %.

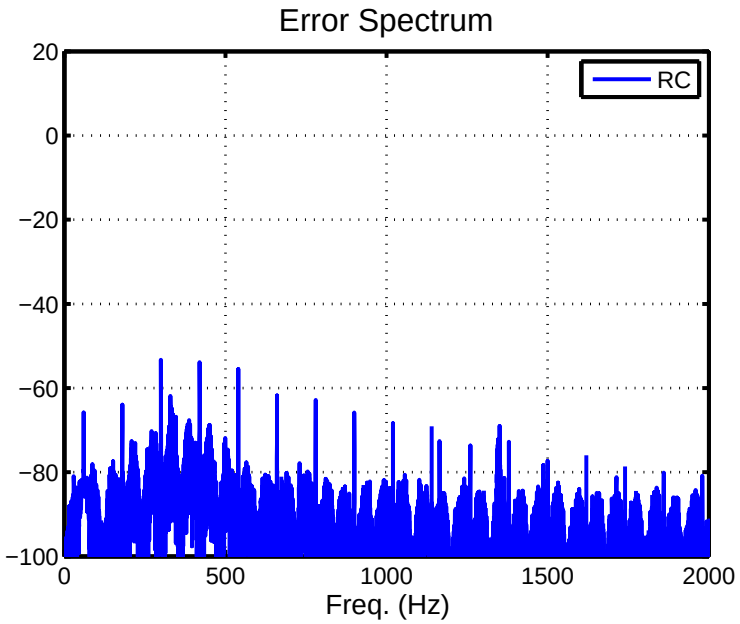

Figure 3.17: Spectrum of the tracking error on the output voltage for Repetitive control

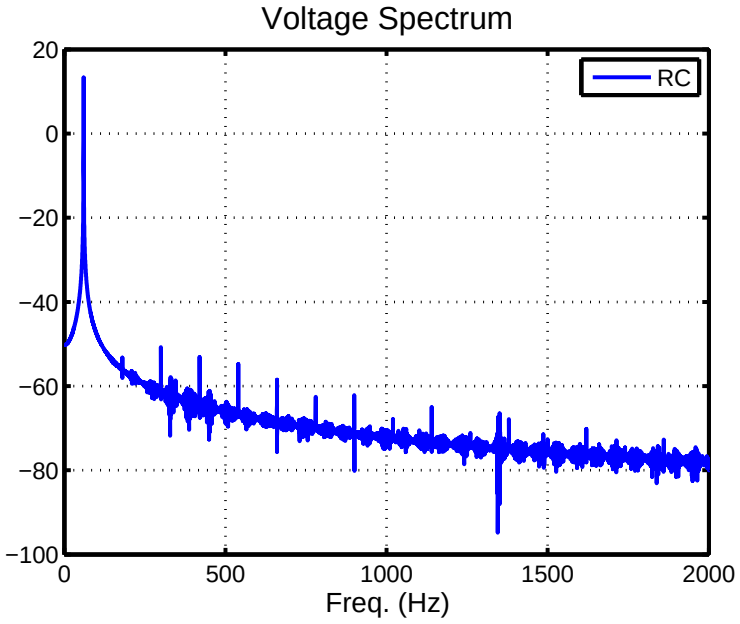

Figure 3.18: Spectrum of the output voltage for Repetitive control (THD=0.14%)

3.4.1.2 Harmonic Resonator

Other than the prototype repetitive control, Wang [WCT09] introduced an intern model type controller for tracking/rejecting signal at specific interested frequency. The idea is to replace the group delay in the positive feedback loop of the repetitive control by peak filter as shown in Figure 3.19. The peak filter in the positive feedback loop provides high loop gain at the interested frequencies while reject the components at other frequencies. The detail analysis and derivation of this IMP type control design is omitted here but can be found in [KT14a, WCT09].

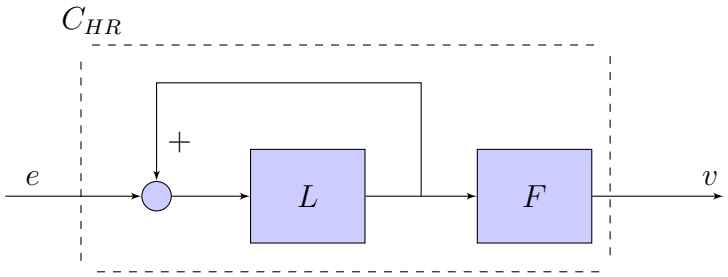

Figure 3.19: Block diagram of the plug-in Harmonic Resonator

One of the advantage of Peak filter design over Repetitive control is that the location of the peak is a design parameter. One can design the peak filter according to the output spectrum of the pre-stabilized system. From Figure 3.6, the output spectrum of the open-loop system shows significant components up to 23th harmonics. We designed the peak filter in this section to have 12 peaks at the odd harmonics from 1-23. And the frequency response of the peak filter is shown in Figure 3.20. Therefore, the harmonic resonator is expected to not only track the 60 Hz AC voltage but also compensate for harmonics from 3rd to 23rd.

Figure 3.21 and 3.22 shows the spectrum of the tracking error and output voltage respectively. The harmonic resonator effectively compensate for the harmonics at the designed frequencies. Since no control action was taken for harmonics higher than 1380 Hz, the THD of the harmonic resonator is not as good

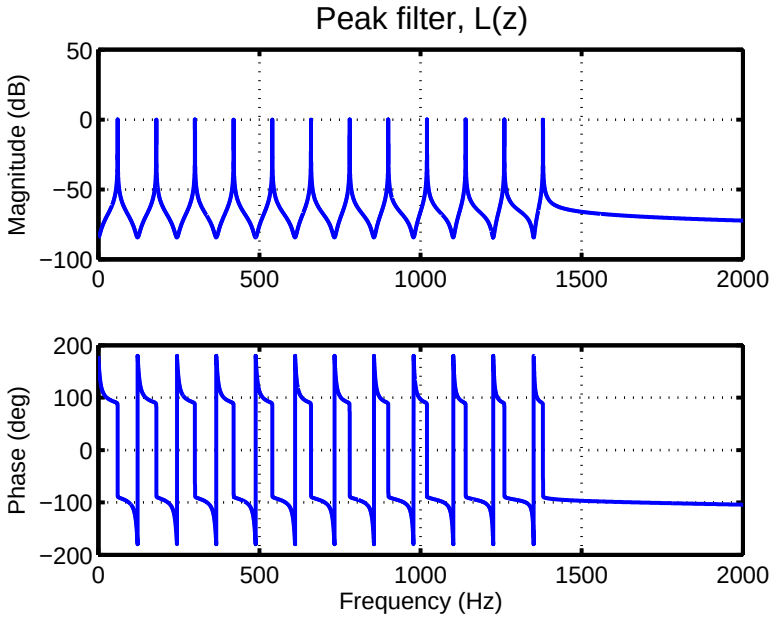

Figure 3.20: Frequency response of the peak filter with 12 peaks at odd harmonics from 1 to 23th

as repetitive control who takes care of harmonics up to the bandwidth of Q-filter. But the harmonic resonator still has THD at 0.15 % which is only 0.01 % higher than the THD for Repetitive control.

3.4.2 Repetitive Control in Rotating Frame (MIMO)

3.4.2.1 Prototype Repetitive Control

In section 3.3, we showed that the performance of PI control in both tracking and harmonics compensation can be improved in DQ rotating frame. Although repetitive control has shown decent performance in fixed frame with THD at 0.14%, the success of PI control in DQ rotating frame gives a motivation for designing repetitive control in DQ coordinate.

However, the power inverter system becomes a MIMO system after applying DQ transformation, as shown in Equation 3.9. Figure 3.12 shows the coupling

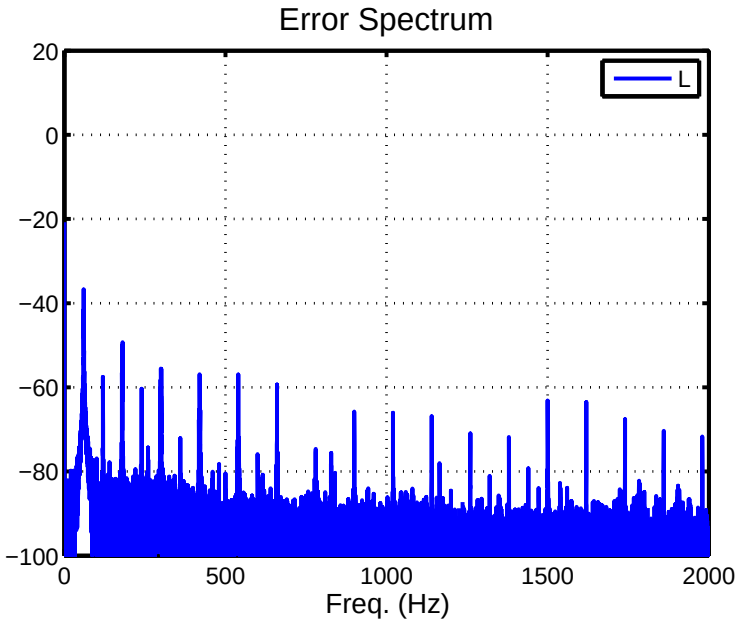

Figure 3.21: Spectrum of the tracking error on the output voltage for Harmonic Resonator

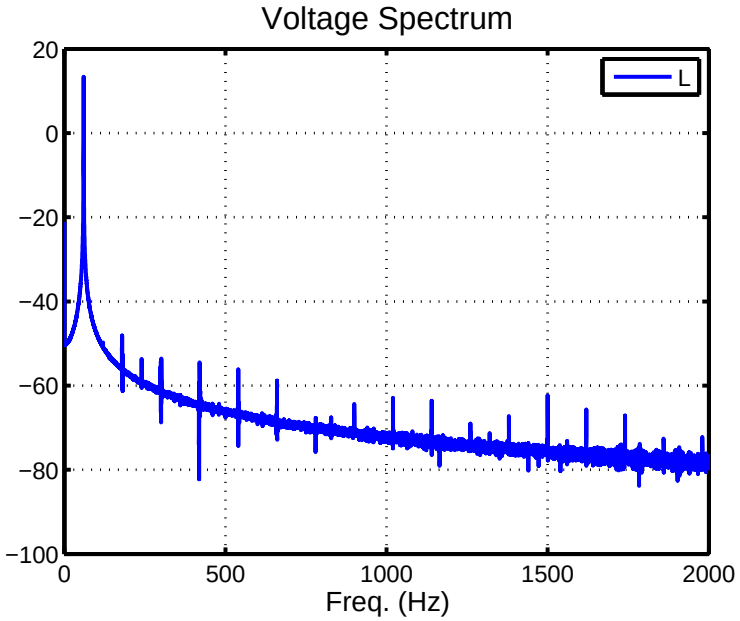

Figure 3.22: Spectrum of the output voltage for Harmonic Resonator (THD=0.15%)

effect for the closed-loop system are too significant to ignore. Therefore, the design of repetitive control for MIMO system introduced in 2.1 will be utilized in this section.

Given the closed-loop MIMO system model,

$$G_{dq}(z) = \begin{bmatrix} \frac{0.0070261(z+12.39)(z^2-1.874z+0.8824)}{(z-0.9441)(z-0.9243)(z^2-1.865z+0.8761)} & \frac{0.0023657(z-0.9006)(z^2-0.2559z+0.4529)}{(z-0.9441)(z-0.9243)(z^2-1.865z+0.8761)} \\ \frac{-0.0026715(z-0.899)(z^2-0.3913z+0.4412)}{(z-0.9441)(z-0.9243)(z^2-1.865z+0.8761)} & \frac{0.0070261(z+12.39)(z^2-1.874z+0.8824)}{(z-0.9441)(z-0.9243)(z^2-1.865z+0.8761)} \end{bmatrix} \tag{3.17}$$

by applying the Smith-McMillan decomposition in section 2.1, the equivalent transfer function matrix of the MIMO system G_{dq} can be calculated

$$M(z) = \begin{bmatrix} \frac{1}{(z-0.9441)(z-0.9243)(z^2-1.865z+0.8761)} & 0 \\ 0 & \frac{(z^2-1.861z+0.6861)(z^2-1.886z+0.8956)}{(z-0.9441)(z-0.9243)(z^2-1.865z+0.8761)} \end{bmatrix} \tag{3.18}$$

and the ZPETC for MIMO system G_{dq} can be further formulated by using Equation 2.11 and 2.12. Figure 3.23 shows the frequency response of the compensated I/O map, $F_{zp}G_{dq}$. The magnitude of the off-diagonal elements of $F_{zm}G_{dq}$ are small enough, -110dB and -200 dB respectively, to be ignored.

Since the compensated I/O map is a decoupled MIMO system with same transfer function at the diagonal terms, we can treat it as two SISO system while implementing the positive feedback loop in repetitive control structure.

Figure 3.24 and 3.25 shows the spectrum of tracking error and output voltage for MIMO repetitive control. The performance is similar to repetitive control in fixed frame, all the harmonics are below -50 dB. But minor improvement can be shown by looking at the THD, repetitive control in fixed frame has THD at 0.14% compared to 0.11% in DQ coordinate.

3.4.2.2 Harmonic Resonator

With the design of ZPETC for MIMO system shown in Chapter 2, the peak filter design for SISO system in [KT14a, WCT09] can also be applied to MIMO system.

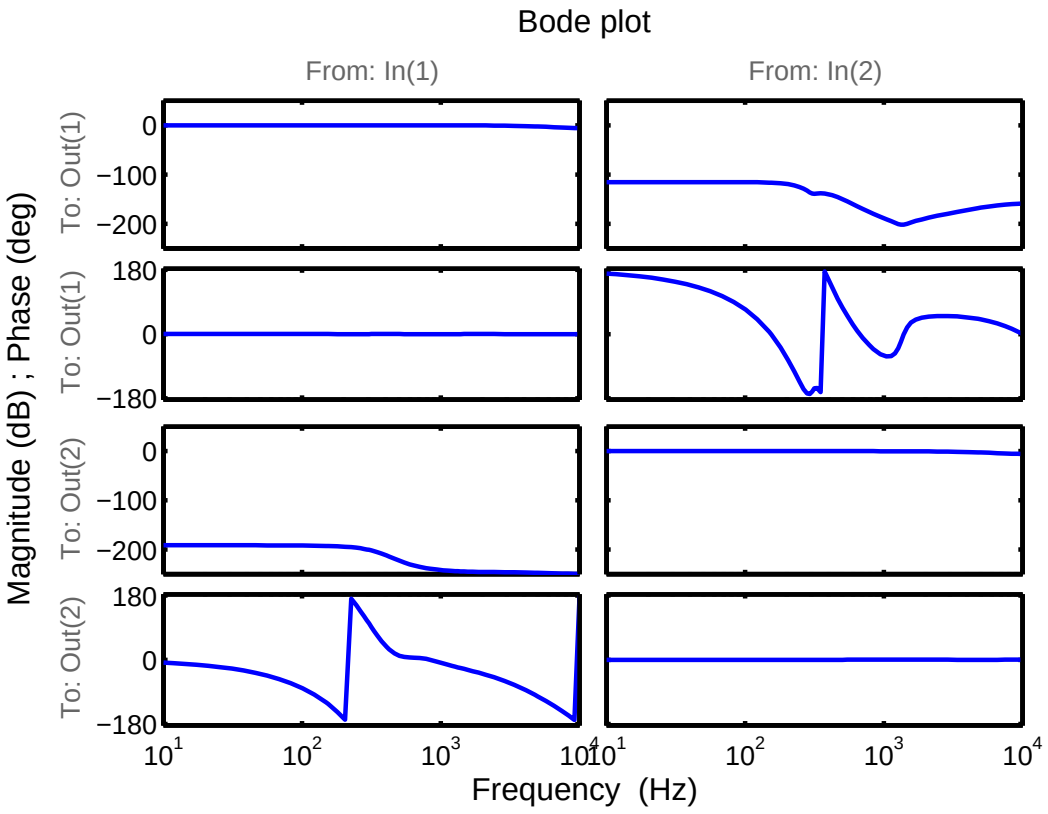

Figure 3.23: Frequency response of compensated I/O map, $F_{zp}G_{dq}$, for MIMO system

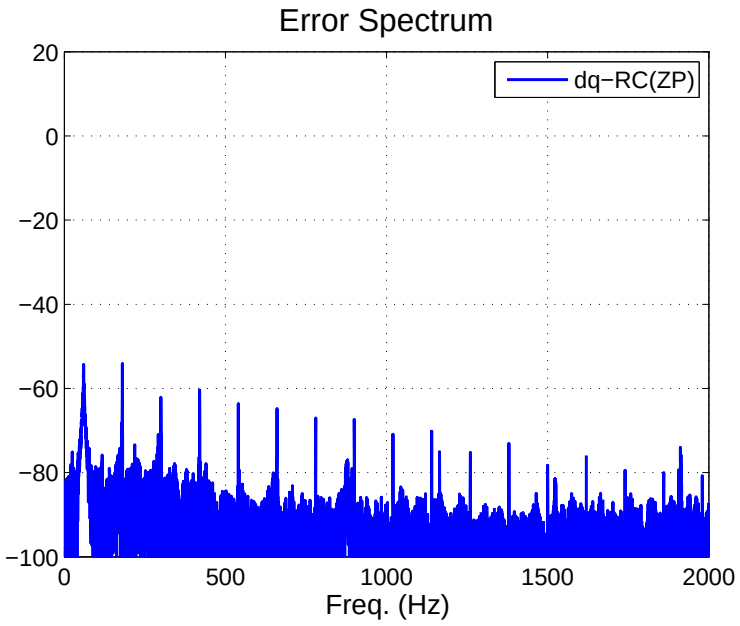

Figure 3.24: Spectrum of the tracking error on the output voltage for MIMO repetitive control

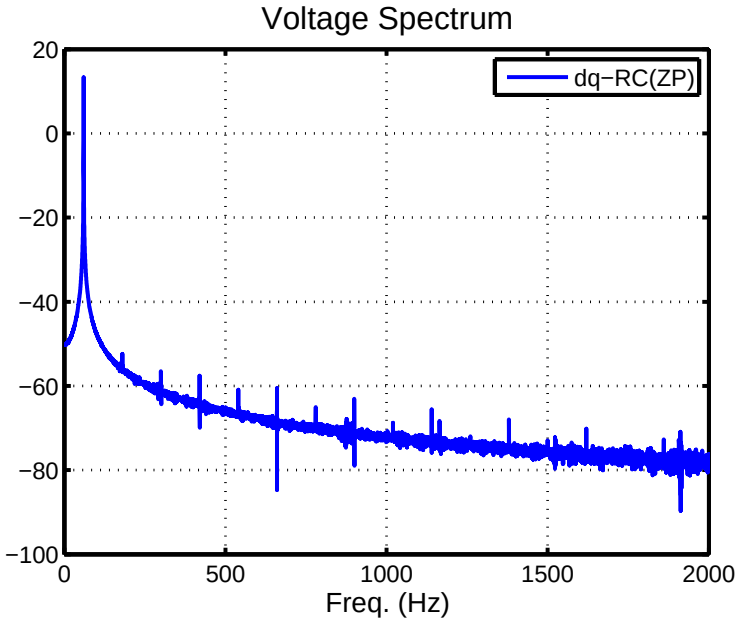

Figure 3.25: Spectrum of the output voltage for MIMO repetitive control (THD=0.11%)

But the frequency gets shifted by 60Hz in rotating frame, the selection on the interested frequency in peak filter will be different. Instead of choosing all the odd harmonics from 1st to 23rd harmonic, we should place the peaks at even harmonics from 2nd to 24th. Although we are using the same number of peaks in the harmonic resonator design, the PI control in rotating frame already takes care of the fundamental harmonic which allows the harmonic resonator to compensate for one more harmonic.

Figure 3.26 and 3.27 shows the spectrum of tracking error and output voltage for MIMO harmonic resonator. The performance is similar to harmonic resonator in fixed frame, all the harmonics are below -50 dB. But minor improvement can be shown by looking at the spectrum at the 25th harmonic. Since the design of peak filter only takes care of the first 12 odd harmonics, the output spectrum of harmonic resonator in fixed frame, shown in Figure 3.22, shows an increase in magnitude from 23rd to 25th harmonic. However, frequency gets shifted by 60Hz in rotating frame, in other words the same number of peaks in harmonic resonator in rotating frame will be able to compensate one more harmonic component than in fixed frame. The experiment results show that harmonic resonator in rotating frame further reduce the THD to 0.13% compared to 0.15% in fixed coordinate.

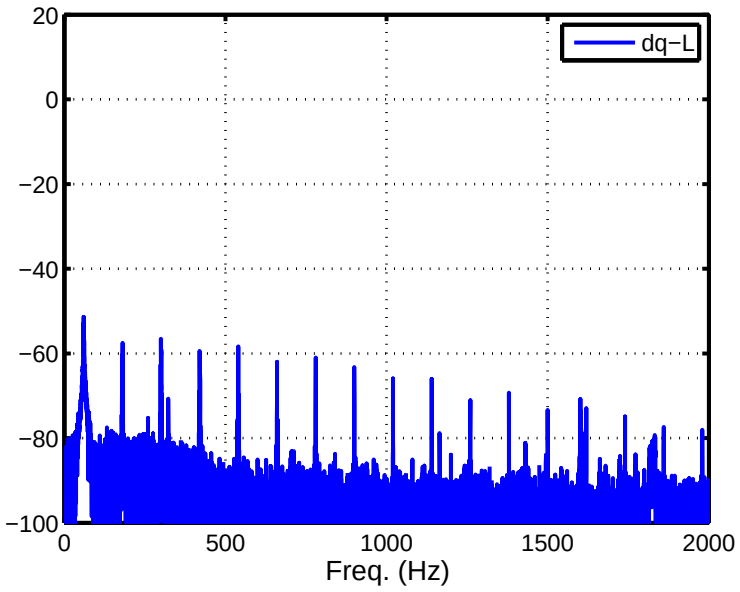

Figure 3.26: Spectrum of the tracking error on the output voltage for MIMO harmonic resonator

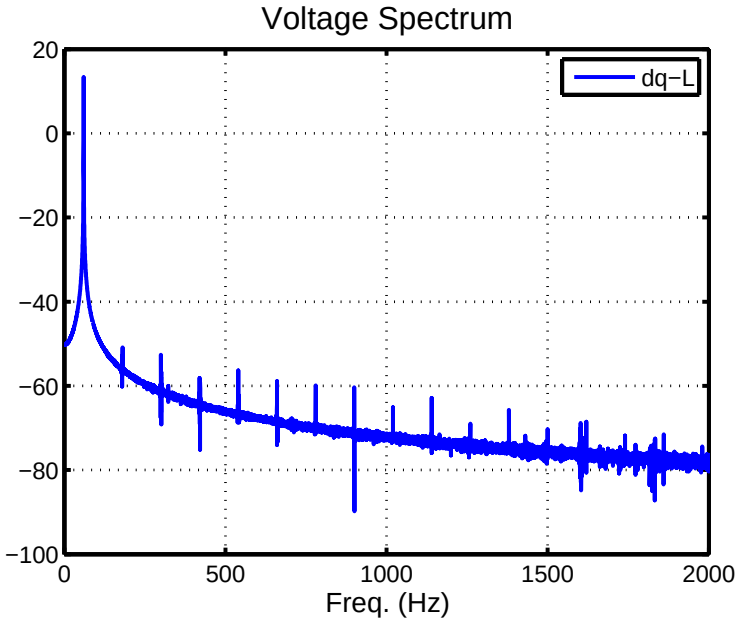

Figure 3.27: Spectrum of the output voltage for MIMO harmonic resonator (THD=0.13%)

3.5 Conclusion

Implementing control within DQ rotating frame is able further improve the overall performance, it not only enhances the tracking of 60Hz AC voltage but also adds more compensation to the harmonics. In either fixed frame or DQ rotating coordinate, repetitive control is able to compensate the harmonics components to a very small extent with THD around 0.1%. Although the MIMO repetitive control does not have significant improvement over SISO repetitive control for power inverter, it could be beneficial for other applications where the control can only be design for MIMO system.

In the next chapter, the control of power rectifier will be discussed. Since the power rectifier is a non-linear system, linearize the system in DQ rotating frame, where all the variables are DC quantities, is beneficial than in fixed frame. Like power inverter, the rectifier becomes a MIMO system in DQ rotating frame where MIMO repetitive control will be applied.

CHAPTER 4

Repetitive Control of Power Rectifier for Harmonic Compensation

In this chapter, the Boost Rectifier will be introduced. The power rectifier shares the same full-bridge switches as shown in 3.1 but the power flows in the opposite direction. The power rectifier converts the AC voltage to a preset DC voltage by controlling the switches. Typical double control loop design is used the inner current loop controls the inductor current in phase with the AC voltage and the outer voltage loop regulates the DC voltage. In this chapter, the control design focus on the inner current loop while the outer voltage loop will be regulated by the same PI control.

A PI control is first used in fixed frame to provide baseline performance. Since PI can only guarantee zero steady sate error for constant reference/disturbance, the tracking error is expected to be significant meaning more reactive current will be circulating through the circuit. Since the power rectifier is a non-linear system, the model has to be linearized prior the design of repetitive control. Instead of linearizing the model in fixed frame, we proposed to convert the model to DQ coordinate before linearization.

In DQ coordinate, the original Single-Input Single-Output (SISO) system becomes Mulit-Input and Multi-Output (MIMO) system coupled by the frequency of the AC voltage. The Repetitive control for Mulit-Input and Multi-Output system introduced in Chapter 2 will be applied to design the repetitive control in D-Q rotating frame for power rectifier.

Different control methods will be implemented to the power rectifier. The simulation results will be presented to compare the performance of tracking error and total harmonic distortion (THD) of the AC current.

4.1 Introduction of Power Rectifier

Traditionally, the rectifiers are developed using diodes to provide DC power. There are several drawback of these designs including poor power factor at input AC current, poor power quality due to injected current harmonics, low efficiency, and large size of AC and DC filters. In several standards [F I93, SSC03], strict requirements of power quality have been announced and are being enforced. Because of all these problems, a new breed of rectifiers using solid state devices such as IGBTs has been developed.

The high frequency switching in full-bridge rectifier is able to reduce the size of AC and DC filters. Besides, the harmonics injected to the current can be compensated by controlling the switches properly. Therefore, the full-bridge rectifier has drawn more and more attentions.

The control objective of the rectifier is to control the inductor current in phase with the AC voltage at minimal THD while regulating the DC voltage at a given level. In this section, the double-loop control structure will be employed where high-bandwidth control of inner current loop and lower bandwidth closed-loop controller on the outer voltage loop will be discussed.

4.2 Modeling of power rectifier

4.2.1 Average model in fixed frame

Figure 4.1 shows the topology of single phase full-bridge boost rectifier. Using the switching defined in Equation 3.2, the input voltage to the rectifier bridge V_{in} is

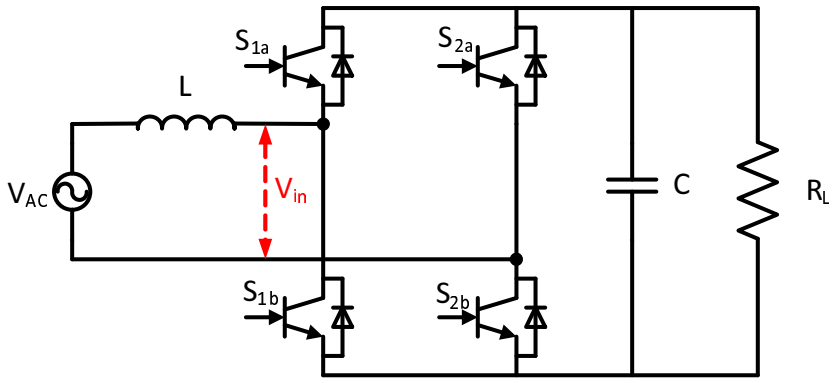

Figure 4.1: Topology of single phase full-bridge boost rectifier

related to the output DC-link voltage V_c as,

$$\begin{aligned} V_{in} &= s_{1a}V_c - s_{2a}V_c \\ &= (s_{1a} - s_{2a})V_c \end{aligned} \tag{4.1}$$

The load current can also be related to the inductor current as,

$$\begin{aligned} I_C + I_{R_L} &= s_{1a}I_L - s_{2a}I_L \\ &= (s_{1a} - s_{2a})I_L \end{aligned} \tag{4.2}$$

The derivative of the capacitor voltage can be written as,

$$C\frac{dV_c}{dt} = I_C \tag{4.3}$$

And the derivative of the inductor current can be written as,

$$L\frac{dI_L}{dt} = V_{AC} - V_{in} \tag{4.4}$$

Combining Equation 4.1-4.4, the following mathematical model can be obtained,

$$\frac{dI_L}{dt} = \frac{V_{AC}}{L} - (s_{1a} - s_{2a})\frac{V_c}{L} \tag{4.5}$$

$$\frac{dV_c}{dt} = -\frac{V_c}{R_L C} + (s_{1a} - s_{2a})\frac{I_L}{C} \tag{4.6}$$

By applying the average operator in Equation 3.7 to Equation 4.5 and 4.6, the average model of single phase boost rectifier can be represented as

$$\frac{d}{dt}\begin{bmatrix} I_L \\ V_c \end{bmatrix} = \begin{bmatrix} 0 & \frac{D}{L} \\ \frac{D}{C} & -\frac{1}{R_L C} \end{bmatrix} \begin{bmatrix} I_L \\ V_c \end{bmatrix} + \begin{bmatrix} \frac{V_{AC}}{L} \\ 0 \end{bmatrix} \tag{4.7}$$

where the control input D is coupled with the states.

In order to linearized the model, the equilibrium points have to be chosen. For the output DC voltage V_c, it is straight forward to choose the desired output DC voltage as the equilibrium point. As for the input voltage V_{AC}, it varies from positive peak to negative peak which makes it difficult to choose a reasonable equilibrium point.

In [SSP03], the equilibrium point of the AC voltage is chosen to be the RMS value. However, the operation range of AC voltage could be far away from that point since the voltage can drop down to negative values so the linearized model will not be accurate in those range. Therefore, we proposed to linearize the model in the DQ coordinate.

4.2.2 Small-signal model in rotating frame

Instead of linearizing the average model in the fixed frame, we proposed to convert the model into DQ coordinate before linearization. Since all the AC variables become DC in DQ frame, the chosen of the equilibrium point will be more meaningful than in fixed frame.

A fictitious circuit has to be added in parallel with the real circuit to enable the DQ transformation for single phase rectifier as shown in Figure 3.8. Assuming all the components in the real and fictitious circuit are 90^o out of phase, then all the AC variables will be orthogonal pairs. The average model includes the real

and fictitious circuit can be rewritten as

$$L\frac{d}{dt}\begin{bmatrix}\boldsymbol{I_{L,a}}\\ \boldsymbol{I_{L,b}}\end{bmatrix} = \begin{bmatrix}\boldsymbol{V_a}\\ \boldsymbol{V_b}\end{bmatrix} - \begin{bmatrix}D_{an,a}\\ D_{an,b}\end{bmatrix}\boldsymbol{V_c} \tag{4.8}$$

$$C\frac{d\boldsymbol{V_c}}{dt} = \frac{1}{2}\begin{bmatrix}D_{an,a} & D_{an,b}\end{bmatrix}\begin{bmatrix}\boldsymbol{I_{L,a}}\\ \boldsymbol{I_{L,b}}\end{bmatrix} - \frac{\boldsymbol{V_c}}{R_L} \tag{4.9}$$

Applying the DQ transformation matrix in Equation 3.8 to Equation 4.8 and 4.9, the average model in DQ coordinate can be derived.

$$L\frac{d}{dt}\begin{bmatrix}\boldsymbol{I_{L,d}}\\ \boldsymbol{I_{L,q}}\end{bmatrix} = \begin{bmatrix}\boldsymbol{V_d}\\ \boldsymbol{V_q}\end{bmatrix} + \omega L\begin{bmatrix}0 & 1\\ -1 & 0\end{bmatrix}\begin{bmatrix}\boldsymbol{I_{L,d}}\\ \boldsymbol{I_{L,q}}\end{bmatrix} - \begin{bmatrix}D_d\\ D_q\end{bmatrix}\boldsymbol{V_c} \tag{4.10}$$

$$C\frac{d\boldsymbol{V_c}}{dt} = \frac{1}{2}\begin{bmatrix}D_d & D_q\end{bmatrix}\begin{bmatrix}\boldsymbol{I_{L,d}}\\ \boldsymbol{I_{L,q}}\end{bmatrix} - \frac{\boldsymbol{V_c}}{R_L} \tag{4.11}$$

Before we linearized the model, we need to find the equilibrium point by letting $\frac{d(\cdot)}{dt} = 0$ in Equation 4.10 and 4.11. Let $\bar{I}_{L,d}$, $\bar{I}_{L,q}$, $\bar{D}_d$, $\bar{D}_q$, $\bar{V}_d$, $\bar{V}_q$, and $\bar{V}_c$ be the equilibrium point. We know the output DC voltage is around $V_{DC,ref}$, so

$$\bar{V}_c = V_{DC,ref} \tag{4.12}$$

Assuming AC voltage is a pure sinusoidal wave with $V_{AC} = V_m\cos(\omega t)$, then

$$V_d = \bar{V}_d = V_m \tag{4.13}$$

$$V_q = \bar{V}_q = 0 \tag{4.14}$$

since inductor current I_L should be in phase with AC voltage V_{AC}, $\bar{V}_q = 0$ implies

$$\bar{I}_{L,q} = 0 \tag{4.15}$$

and we have

$$0 = \bar{V}_d + \omega L\bar{I}_{L,q} - \bar{D}_d \tag{4.16}$$

$$0 = \bar{V}_q - \omega L\bar{I}_{L,d} - \bar{D}_q \tag{4.17}$$

$$0 = \frac{1}{2}\left(\bar{D}_d\bar{I}_{L,d} + \bar{D}_q\bar{I}_{L,q}\right) - \bar{V}_c \tag{4.18}$$

By solving Equation 4.12- 4.18, we have the equilibrium points

$$\bar{I}_{L,d} = 2\frac{\bar{V}_c^2}{R_L \bar{V}_d} \tag{4.19}$$

$$\bar{D}_d = \frac{\bar{V}_d}{\bar{V}_c} \tag{4.20}$$

$$\bar{D}_q = -2\frac{\omega L \bar{V}_c}{R_L \bar{V}_d} \tag{4.21}$$

Defining

$$\tilde{x} = \begin{bmatrix} \boldsymbol{I_{L,d}} - \overline{\boldsymbol{I_{L,d}}} \\ \boldsymbol{I_{L,q}} - \overline{\boldsymbol{I_{L,q}}} \\ \boldsymbol{V_c} - \overline{\boldsymbol{V_c}} \end{bmatrix} \tag{4.22}$$

$$\tilde{u} = \begin{bmatrix} D_d - \overline{D_d} \\ D_q - \overline{D_q} \end{bmatrix} \tag{4.23}$$

The small signal model can be written as follows,

$$\dot{\tilde{x}} = A\tilde{x} + B\tilde{u} \tag{4.24}$$

where

$$A = \begin{bmatrix} 0 & \omega & -\frac{\overline{D_d}}{L} \\ -\omega & 0 & -\frac{\overline{D_q}}{L} \\ \frac{\overline{D_d}}{2C} & \frac{\overline{D_q}}{2C} & -\frac{1}{R_L C} \end{bmatrix} \tag{4.25}$$

$$B = \begin{bmatrix} -\frac{\overline{\boldsymbol{V_c}}}{L} & 0 \\ 0 & -\frac{\overline{\boldsymbol{V_c}}}{L} \\ \frac{\overline{\boldsymbol{I_{L,d}}}}{2C} & \frac{\overline{\boldsymbol{I_{L,q}}}}{2C} \end{bmatrix} \tag{4.26}$$

4.3 Control Design for Inner Current Loop

Figure 4.2 shows the double loop control structure used in this section, the outer voltage loop controller, PI control, regulates the DC link voltage by changing the magnitude of the desired inductor current. The inner loop controller drives the PWM generator to track the current profile.

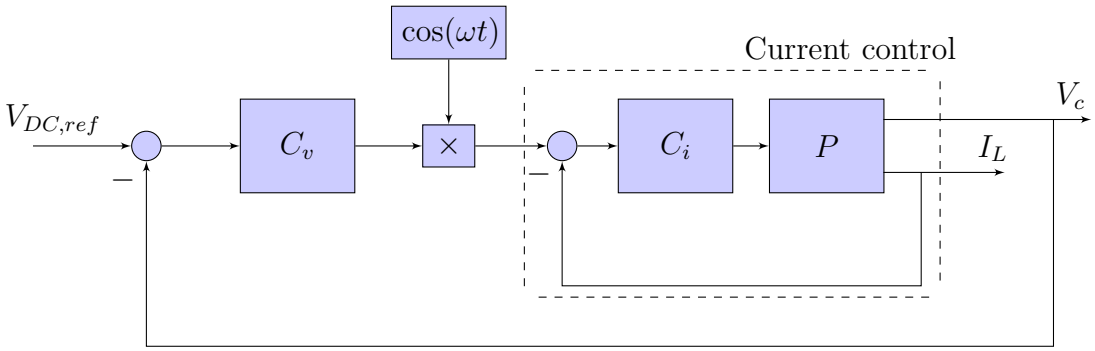

Figure 4.2: Block diagram of the double loop control structure

The control design in this section focus on the inner loop controller while the outer loop voltage controller will be PI control for all cases.

4.3.1 AC Current Tracking with PI Control

In this section, different inner loop controller is used in the fixed frame to control the power rectifier to track AC current with small THD while regulating the DC voltage at a given reference.

A simulation on the non-linear average model, Equation 4.7, is used to verify the performance of different controller.

4.3.1.1 Fixed Frame Design

A PI control is first tuned to control the power rectifier to track the AC current generated from the outer voltage loop as shown in Figure 4.2.

Figure 4.3 and 4.4 shows the spectrum of the tracking error and the AC current respectively. It is evident that the PI control has error components at 60 Hz, meaning the phase of the AC current is not in phase with the AC voltage.

In order to ensure the AC current is in phase with the AC voltage, a PI control in DQ rotating frame will be introduced in the next section.

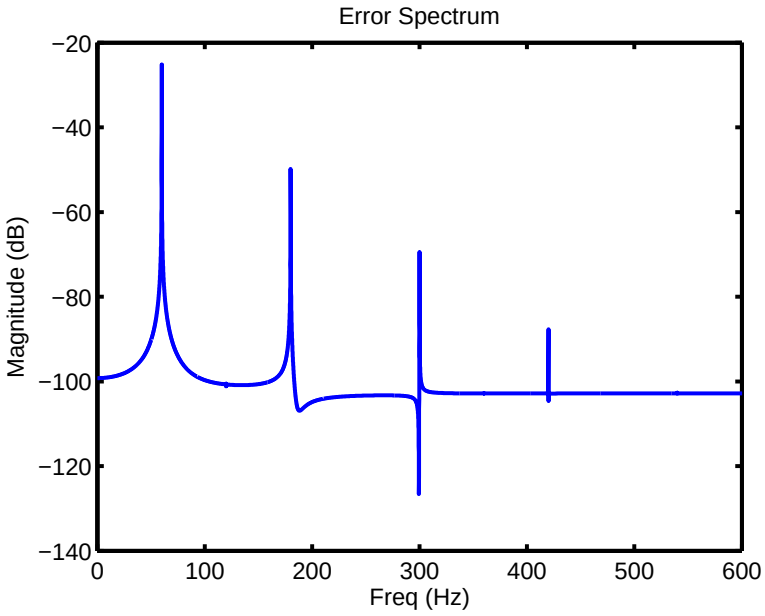

Figure 4.3: Spectrum of the tracking error on the AC current for PI control in fixed frame

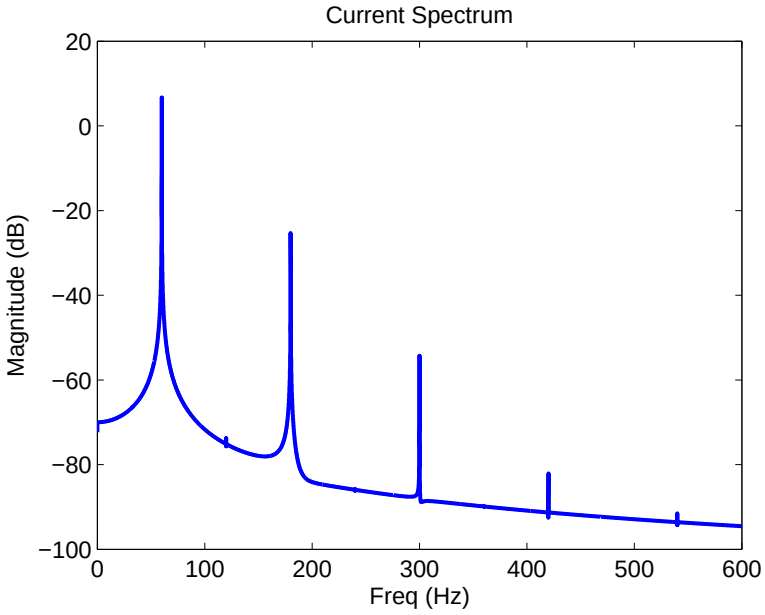

Figure 4.4: Spectrum of the AC current for PI control in fixed frame(THD=2.61%)

4.3.1.2 Rotating Frame Design

By following the steps in section 4.2.2, the small-signal model in DQ coordinate can be derived. The operating condition of the power rectifier is chosen to be:

- $V_{DC,ref} = 300$ (volt)
- $V_{AC} = 120\cos(\omega t)$ (volt)

Figure 4.5 shows the frequency response of the linearized model, it is a MIMO system with significant coupling dynamics on both states.

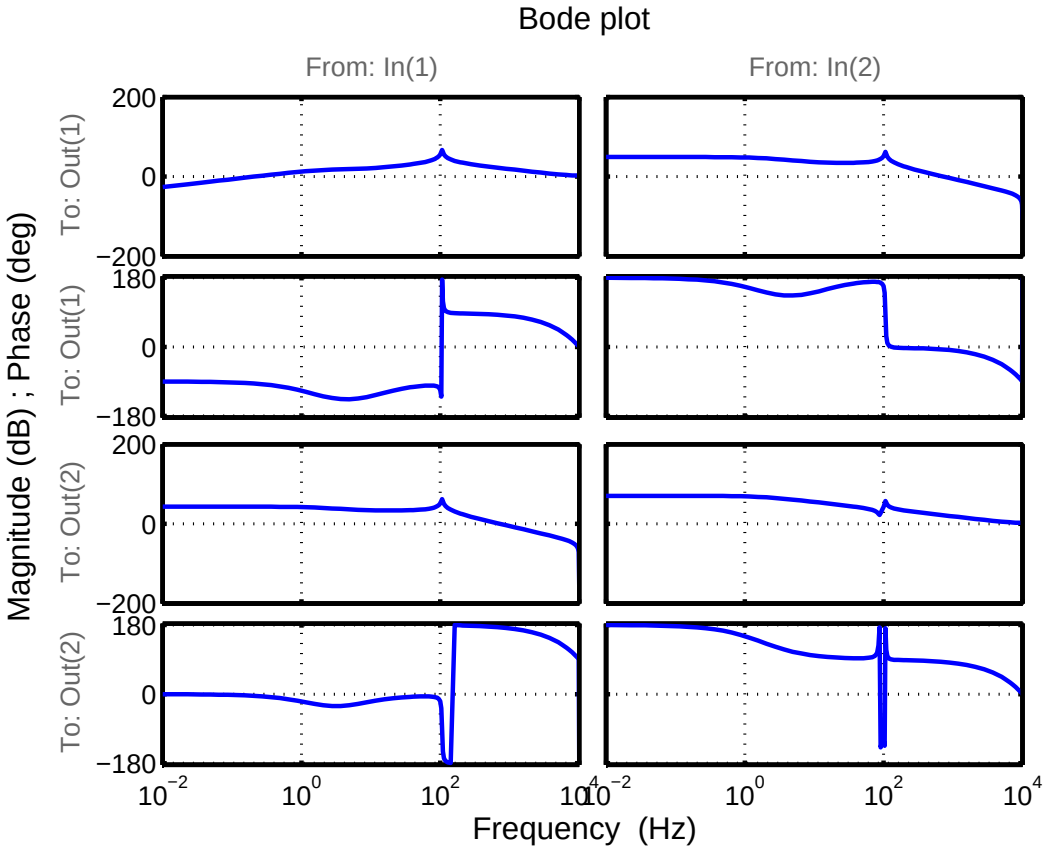

Figure 4.5: Frequency response of the open loop linearized rectifier model in DQ coordinate

In this section, a PI control is used to form a closed-loop system that provides zero steady state error so that the AC current will be in phase with AC voltage. The frequency response of the closed loop system is shown in Figure 4.6.

The simulation results in Figure 4.7 and 4.8 show that the PI control in DQ coordinate makes the AC current in phase with the AC voltage. Although the

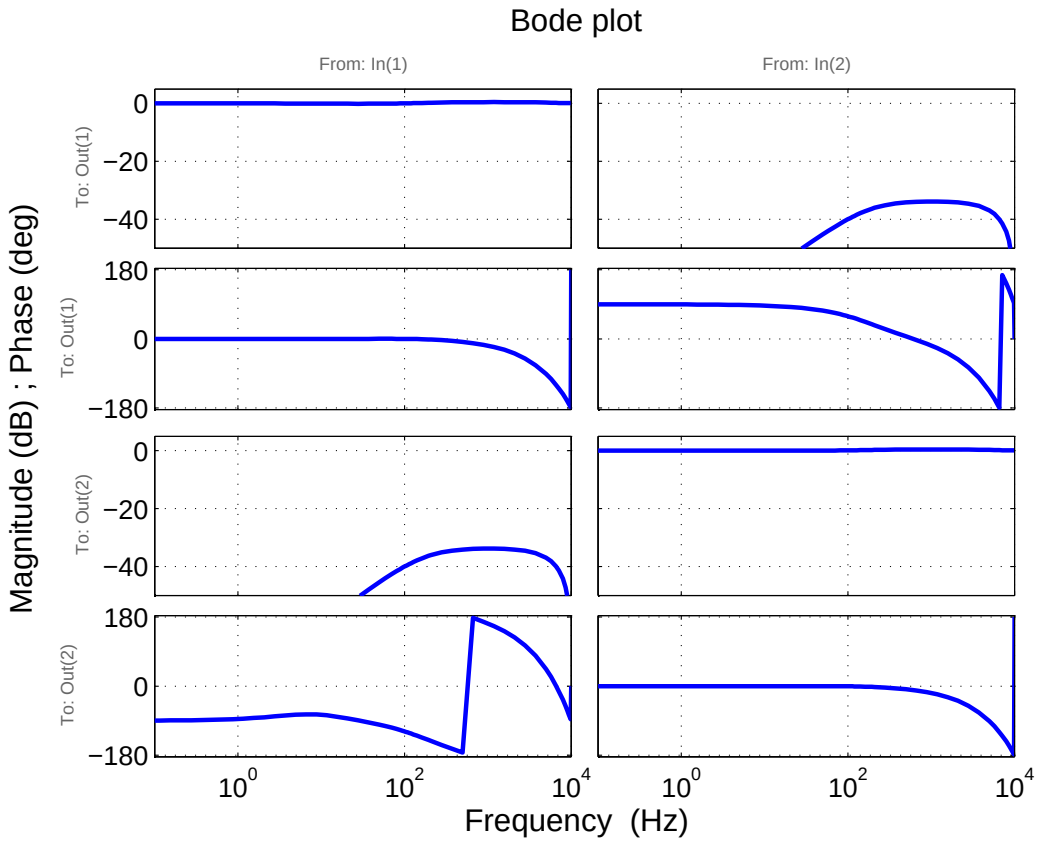

Figure 4.6: Frequency response of the closed loop linearized rectifier model in DQ coordinate

3rd, 5th, and 7th harmonics still have significant components, the total harmonic distortion is reduced to 1.2% compared to 2.4% with PI control in fixed frame.

The PI control has infinite loop gain at 0 Hz in DQ coordinate which corresponds to 60 Hz in fixed frame. In the next section, a repetitive control with infinite loop gain at all harmonics will be introduced to compensate for the odd harmonics shown in Figure 4.7 and 4.8.

4.3.2 Harmonic Reduction by Repetitive Control in Rotating Frame

As shown in Figure 4.6, the power rectifier becomes a MIMO system in DQ coordinate. Although the coupling effect for the closed-loop system is not significant,

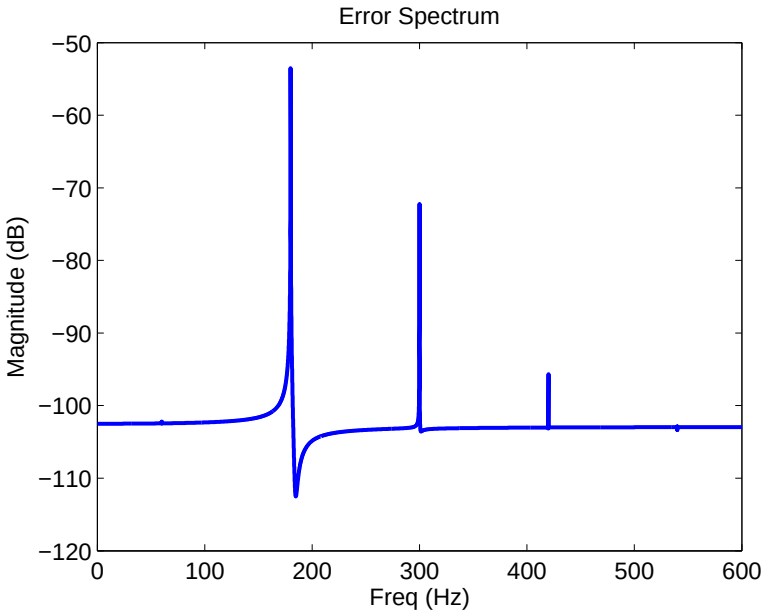

Figure 4.7: Spectrum of the tracking error on the AC current for PI control in DQ frame

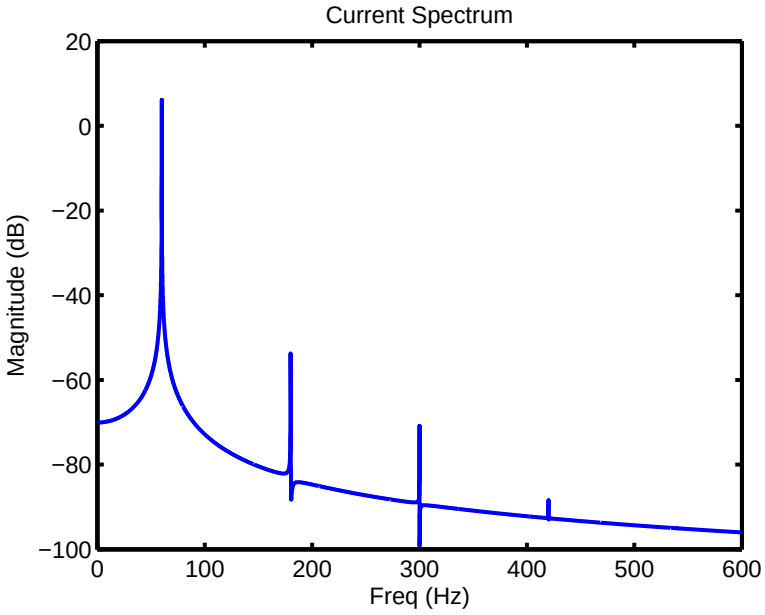

Figure 4.8: Spectrum of the AC current for PI control in DQ frame(THD=1.2%)

it still needs to be compensated in designing repetitive control. The design of repetitive control for MIMO system introduced in Chapter 2 will be used in this

section.

By applying the Smith-McMillan decomposition, the equivalent transfer function matrix of the MIMO system Gr_{dq} can be calculated. And the ZPETC, Fr_{zp}, for MIMO system can be further formulated by using Equation 2.11 and 2.12. Figure 4.9 shows the frequency response of the compensated I/O map for MIMO system, the magnitude of the coupling terms are below -100 dB. Therefore, the compensated I/O map can be treated as a MIMO system with two decoupled SISO system. According to Equation 2.15, the two decoupled SISO system will be identical, so the prototype repetitive control can be implemented directly.

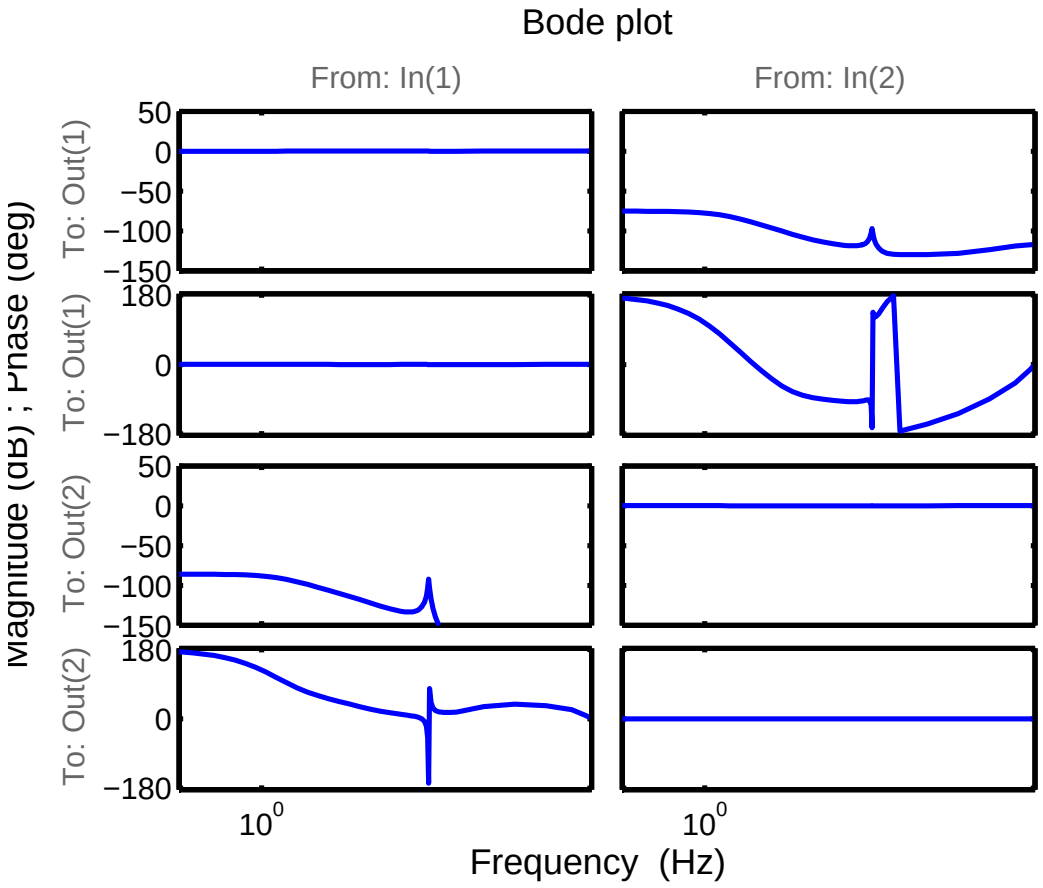

Figure 4.9: Frequency response of the compensated I/O, $Fr_{dq}Gr_{dq}$, for MIMO system

Figure 4.10 shows the spectrum of AC current for MIMO repetitive control.

The performance is better than PI control in either fixed frame or DQ frame, all the harmonics are compensated with superior THD = 0.006%.

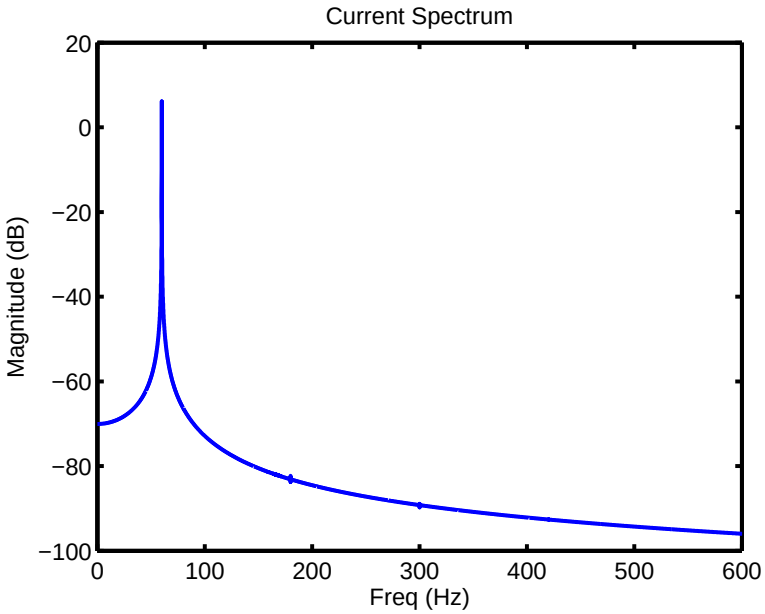

Figure 4.10: Spectrum of the AC current for Repetitive control in DQ frame(THD=0.006%)

4.3.3 Simulation Results

Figure 4.11 shows the simulation results in DC voltage for different inner loop controllers. The DC voltage of PI control oscillates around the reference DC voltage in both fixed frame and rotating frame while the oscillation is negligible for repetitive control.

As shown in Table 4.1, the Repetitive control has superior THD at 0.006% compared to 2.4% and 1.2% for PI control in fixed frame and DQ frame respectively. As the power factor is defined

$$PF = \frac{1}{\sqrt{1+THD^2}} = \frac{I_{1,rms}}{I_{rms}} \tag{4.27}$$

the efficiency of the power rectifier can be reached to almost 100 % by implement-

	THD
PI in fixed frame	2.4%
PI in DQ frame	1.2%
RC in DQ frame	0.0006%

Table 4.1: Total Harmonic Distortion of different inner currnet loop controller

ing repetitive control in DQ coordinate for the inner current loop.

4.4 Conclusion

The proposed repetitive control for MIMO system in Chapter 2 enables the design of repetitive control for power converters in DQ coordinate. In this chapter, we have shown that the Repetitive control in DQ coordinate for power rectifier has superior performance with THD = 0.006% corresponds to almost 100% in power conversion without considering switching loss, heat loss, and etc.

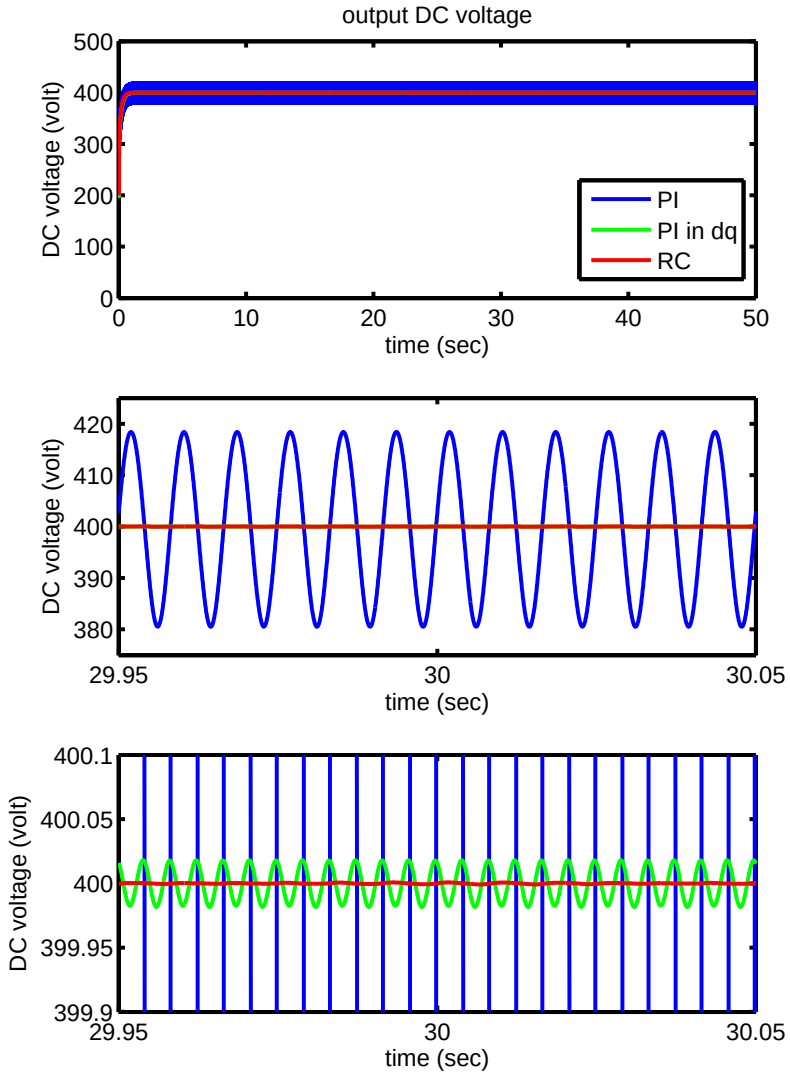

Figure 4.11: DC voltage for PI control in fixed frame, DQ frame, and Repetitive control in DQ coordinate

CHAPTER 5

Inversion Based Iterative Learning Control for Precision Motion Control

5.1 Introduction

Iterative learning control (ILC) is a commonly used control methodology for applications that execute the same task multiple times [BTA06, ACM07, KT04]. For these systems, the tracking reference has the same length and keeps unchanged from one run to the next. This feature implies that the error signal from the previous run has rich information. The objective of ILC is to minimize the tracking error by taking advantage of the error information from the previous runs to anticipate the control signal that can provide high-performance tracking result. In various industrial applications that execute repeated operation, ILC has shown its effectiveness on improving the performance. This includes industrial robots [Tay04, GN01], computer numerical control machine [KT04], wafer stage motion systems [BA08], and chemical processing [CQL04].

The learning filter in ILC determines the performance of the algorithm, it decides how the past information will be used and which part of the information will be learned. The proportional type (P-type) and proportional-derivative type (PD-type) ILC are very popular among other learning filters [CM02], since they do not require much knowledge about the system. However the tuning process for these two learning filters could be tedious and the learning process has to be reset whenever the parameters are adjusted. On the other hand, there are

several popular model-based ILC algorithms such as model inversion methods, H_∞ methods, and quadratically optimal design methods [BTA06]. Model inversion methods use the inverse of the system dynamic as the learning function. H_∞ methods formulate the problem into linear fractional transformation form and solves the model mismatch problem. In quadratically optimal design methods, the learning function is defined in the lifted domain that minimizes the quadratic cost criterion for the next iteration where the estimation is based on the knowledge of the system model. The above model-based algorithms utilize the system model in different manner but the performance is mainly determined by the closeness of the model to the actual system.

For all different types of ILC algorithm, the idea behind designing or tuning the learning function is to approximate the inverse of the system dynamic so that the control law can be updated towards the optimal control for a given reference. In the case of P-type and PD-type ILC, the approximation is made by tuning proportional and derivative gains which constitutes a first order learning filter. A first order filter may be able to capture the trend of the system dynamic while high order dynamics could be missing which limits the convergence rate and the steady state error for P-type and PD-type ILC.

In model-based ILC algorithms, learning function is obtained from the knowledge of system dynamics. Although different algorithm formulates the learning function differently, the main idea is to find a learning filter that is closest to the inverse of the system dynamics. For model inversion based ILC, the learning function is simply chosen to be the inverse of the system dynamics. If the system dynamic is invertible, the tracking error should converge to zero within one iteration. While the system has non-minimum phase zero, the inversion of the system will become an unstable filter. In the literature, there are several methods that approximate the inversion of non-minimum phase system. In time domain, zero-phase-error tracking controller (ZPETC) [Tom87, TT87, KT14b], zero-magnitude-

error tracking controller (ZMETC) [RPL09], and direct inversion [CT14] have been used to invert non-minimum phase system. In frequency domain, Model-less Inversion-Based Iterative Control (MIIC) [KZ08] has been applied to inverse the dynamic of atomic force microscope.

In this chapter, a data-based dynamic inversion method in frequency domain is proposed to approximate the inverse of system dynamic. It utilizes the information from testing data in frequency domain to construct the learning function which not only reduces the unmodeled dynamics but also gets around the issue of inverting non-minimum phase system. All the aforementioned inversion methods are implemented on a linear motor for tracking a 50 Hz triangle wave. The performance is compared in terms of convergence rate and final converged error.

The remainder of this chapter is organized as follows: In Section 5.2, the model inversion-based ILC algorithm will be introduced along with the stability and performance analysis. Section 5.3 studies different types of non-minimum phase inversion method including model-based and data-based. In section 5.4, the simulation results are shown to compare the performance of inversion based iterative learning control algorithm with different inversion method for a 50 Hz triangle wave and a non-circular piston profile. In addition, all the control algorithms are implemented in real-time to control the linear motor system. The experimental results are shown in section 5.5. Model-based ILC with ZPETC is implemented on a CNC lathe to perform real cutting. The cutting results are presented in section 5.6

5.2 Inversion Based Iterative Learning Control Algorithm

Consider the feedback control system shown in figure 5.1. where P represents the open-loop plant model and C is a pre-existing stabilizing controller which is designed based on some predetermined performance criteria.

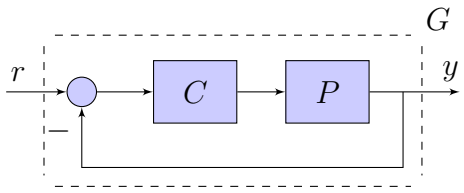

Figure 5.1: Stable Feedback Controlled system

This stable closed-loop system can be represented as G, where

$$G = \frac{CP}{1 + CP} \tag{5.1}$$

The control objective of G is to follow any given reference input. While the system operates repeatedly on a finite length of reference input, the tracking error should remain the same if no disturbances are considered. If the control law can take advantage of using the information from previous iterations, the tracking error is expected to converge.

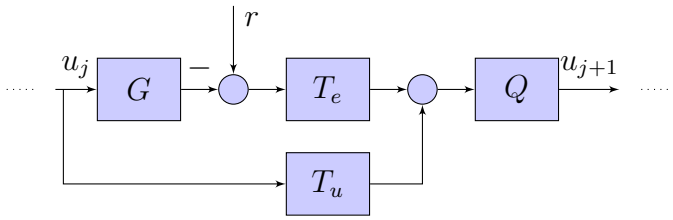

Figure 5.2: General Iterative Learning Control system, where G is the stable closed-loop plant, T_e and T_u are the learning function for error and control respectively, and Q is the low-pass filter

Figure 5.2. shows the block diagram of the generic ILC update law, where r is the reference input, u_j is the control at j^{th} iteration, G is the stable closed-loop system, T_e and T_u are the learning function for error and control respectively, and

Q is the low-pass filter. And r, u_j, and y_j are vectors

$$r = [r(1) \ \ldots \ r(N)]^T$$
$$u_j = [u(0) \ \ldots \ u(N-1)]^T$$
$$y_j = [y(d) \ \ldots \ y(d+N-1)]^T$$

where N is the number of samples in the reference profile; d is the relative order of the pre-stabilized system G.

Choosing $T_u(q) = I$, the ILC control update law in Figure 5.2 can be written as,

$$u_{j+1} = Q(q)\left[u_j + T_e(q)\left(r - y_j\right)\right] \tag{5.2}$$

where $Q(q)$ and $T_e(q)$ are $N \times N$ matrices.

If $N = \infty$, we can apply one-sided Z transform to Equation 5.2. Then z-domain representation of the update law can be obtained,

$$u_{j+1}(k) = Q(z)\left[u_j(k) + T_e(z)\left(r(k) - y_j(k)\right)\right] \tag{5.3}$$

the ILC system in Equation 5.3 is asymptotically stable if [NG02],

$$\left|Q(z)\left(1 - T_e(z)G(z)\right)\right| < 1 \tag{5.4}$$

and the asymptotic error is,

$$e_\infty(z) = \frac{1 - Q(z)}{1 - Q(z)\left[1 - T_e(z)G(z)\right]} r(z) \tag{5.5}$$

One way to satisfy the stability condition in Equation 5.4 is to choose the error learning function, T_e, to be the inverse of $G(z)$. If the exact system inversion can be obtained such that

$$T_e(z)G(z) = 1 \tag{5.6}$$

then the error will converge to

$$e_\infty(z) = (1 - Q(z))\, r(z) \tag{5.7}$$

meaning that the tracking error of the inversion based ILC algorithm will converge to zero with $Q(z) = 1$.

However, the error will not converge to zero because there exists unmodelled dynamics in the system, a low-pass Q-filter is necessary to enhance the robustness. Also the dynamic inversion is not realizable if the system have non-minimum phase zero. The stable closed-loop system G in equation 5.1 can be defined as

$$G(z^{-1}) = \frac{CP}{1 + CP} = z^{-d} \frac{B^+(z^{-1})B^-(z^{-1})}{A(z^{-1})} \tag{5.8}$$

where d represents a known delay, $B^+(z^{-1})$ includes stable zeros, and $B^-(z^{-1})$ are unstable zeros. The inversion of the unstable zeros becomes $\frac{1}{B^-(z^{-1})}$ which is a unstable filter. In order to get around this issue, different stable approximate techniques will be introduced in the next section.

5.3 Non-Minimum Phase Dynamic Inversion

In this section, different stable approximate model inversion methods will be applied for learning function T_e including ZPETC, ZMETC, approximated direct inversion, Time reversal phase cancellation, and the proposed frequency domain inversion. In order to enhance the robustness of the leaning function, a linear phase low-pass Q-filter will be applied with the above stable approximate model-inversion method. So that the learning function will be,

$$T_e(z) = Q(z)F_x(z) \tag{5.9}$$

where F_x denotes different stable approximate methods.

The Q-filter is a linear phase low-pass FIR filter. Because of the ILC update

law is implemented between iterations, the anti-causal filtering can be realized by shifting the pre-filtered signal with the group delay of the Q-filter. Also the preview shift can be utilized to compensate the delay caused by the plant itself. In this way, the ILC update law can anticipate the high-performance control signal.

5.3.1 Model Based

5.3.1.1 Zero Phase Error Tracking Control (ZPETC)

The ZPETC technique approximates the plant inversion by cancelling the phase effect from the unstable zeros while shitting the dc gain to unity. When utilizing ZPETC technique [Tom87] to inverse the non-minimum phase dynamic system as shown in Eq 5.8, the plant inversion becomes:

$$F_{zp}(z) = z^{-n_u} \frac{A(z^{-1})}{B^{+}(z^{-1})} \frac{[B^{-}(z^{-1})]^{*}}{b} \tag{5.10}$$

where b maintains the DC-gain of $F_{zp}G$ at 1, n_u is the order of $B^{-}(z^{-1})$, and z^{-n_u} makes F_{zp} casual.

By taking the complex conjugate of the unstable zeros, it converts the unstable filter $B^{-}(z^{-1})$ into a stable filter. Also the multiplication of $B^{-}(z^{-1})$ and its complex conjugate cancels out the phase, therefore the overall transfer function, $F_{zp}G$, becomes

$$F_{zp}(z)G(z) = z^{-n_u-d} \frac{B^{-}(z^{-1})\,[B^{-}(z^{-1})]^{*}}{b} \tag{5.11}$$

Although the ZPETC uses a constant b to maintain the dc-gain at unity, the magnitude of the overall transfer function changes with frequency. The location of the unstable zeros determine the magnitude of the overall transfer function [RPL09].

Assume the system has only one unstable zero, and it is at location $z = a$,

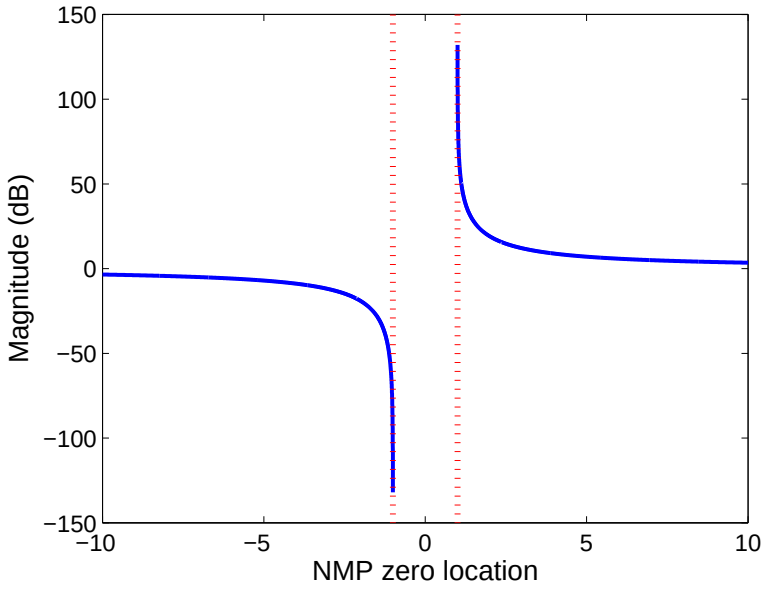

Figure 5.3: Magnitude of overall transfer function, $F_{zp}G$, at nyquist frequency with different NMPZ location

$$B^{-}(z^{-1}) = 1 - az^{-1},\ |a| > 1 \tag{5.12}$$

the overall transfer function can be written as,

$$\begin{aligned} F_{zp}(z)G(z) &= \frac{(z-a)(-az+1)}{z^2(1-a)^2} \\ &= \frac{(e^{j\omega}-a)(-ae^{j\omega}+1)}{e^{j2\omega}(1-a)^2} \\ &= \frac{\cos(\omega)(1+a^2-2a\cos(\omega))}{(1-a)^2} \\ &\quad + j\frac{-\sin(\omega(1+a^2-2a\cos(\omega)))}{(1-a)^2} \end{aligned} \tag{5.13}$$

Figure 5.3 shows the magnitude of the overall transfer function, $F_{zp}G$, at nyquist frequency for different non-minimum phase zero (NMPZ) locations.

The overall transfer function, $F_{zp}G$ has magnitude approaching to infinity

while the NMPZ is around 1, and the magnitude converges to unity while the NMPZ goes farther away from unit circle. Therefore, when the NMPZ is positive and close to unit circle, the magnitude of the overall transfer function gets larger at high frequency which degrades the performance and might result in unstable filter.

5.3.1.2 Zero Magnitude Error Tracking Control (ZMETC)

Instead of cancelling out the phase of the system dynamics, the concept of ZMETC is to approximate the unstable zeros by its magnitude. The ZMETC of system G in equation 5.8 can be written as,

$$F_{zm}(z) = \frac{A(z^{-1})}{B^{+}(z^{-1})\,[B^{-}(z^{-1})]^{*}} \tag{5.14}$$

and the overall transfer function will be,

$$F_{zm}(z)G(z) = z^{-n_u}\frac{B^{-}(z^{-1})}{[B^{-}(z^{-1})]^{*}} \tag{5.15}$$

Since the complex conjugate of a filter will only change the phase, the magnitude of the overall transfer function across all frequencies will be unity. And the resulted overall transfer function by applying ZMETC technique [RPL09] becomes an IIR filter with distorted phase.

Again, assume the system has one unstable zero at $z = a$ as written in Equation 5.12. The overall transfer function $F_{zm}G$ in Equation 5.15 can be written as,

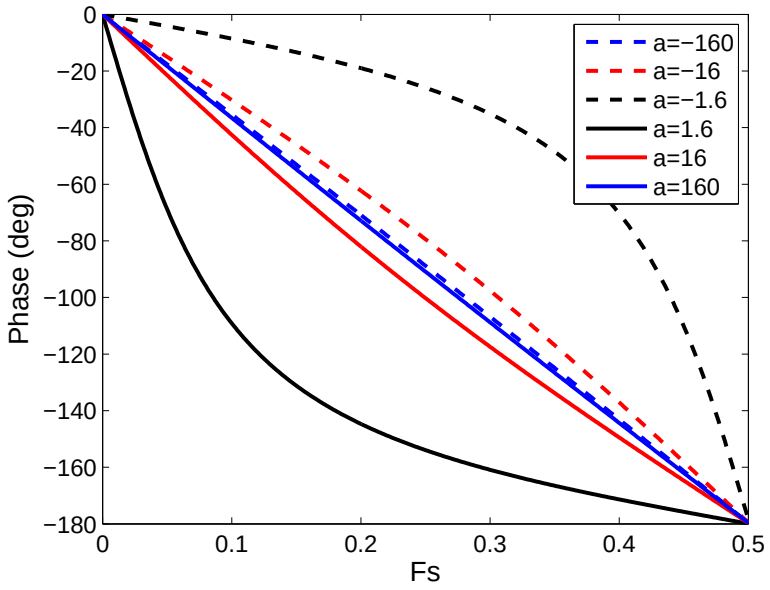

Figure 5.4: Phase of overall transfer function, $F_{zp}G$, up to nyquist frequency with different NMPZ location

$$\begin{aligned} F_{zm}(z)G(z) &= \frac{z-a}{-az+1} \\ &= \frac{e^{j\omega}-a}{-ae^{j\omega}+1} \\ &= \frac{(1+a^2)\cos(\omega)-2a}{1+a^2-2a\cos(\omega)} \\ &\quad + j\frac{(1-a^2)\sin(\omega)}{1+a^2-2a\cos(\omega)} \end{aligned} \tag{5.16}$$

In Figure 5.4, the phase of overall transfer function $F_{zm}G$ with different NMPZ location is presented. While the NMPZ is far away from the unit circle, as shown in blue lines, the phase distortion is almost linear with respect to frequency. As the NMPZ is close to unit circle, the phase becomes more non-linear.

In both cases, a one step look-ahead could be applied to the overall transfer function to compensate for the phase. The resulted overall transfer function would have almost zero phase if the NMPZ is far away from the unit circle. For the

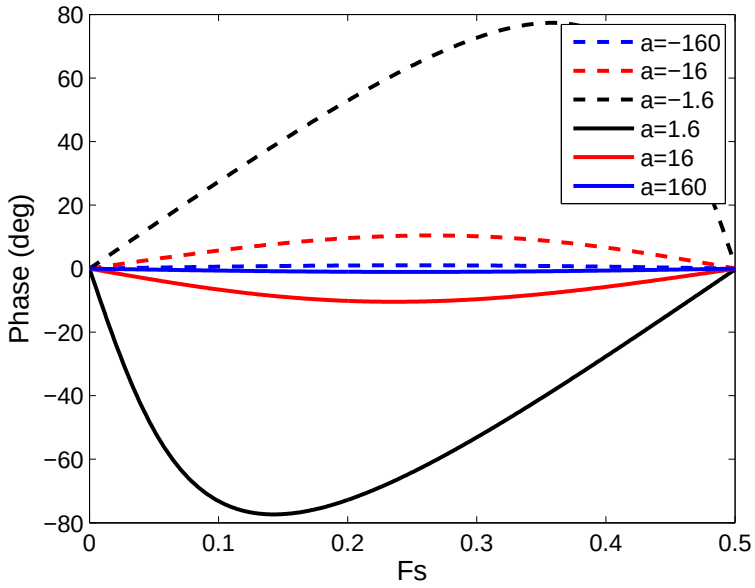

Figure 5.5: Phase of overall transfer function, $z^q F_{zp} G$, up to nyquist frequency with different NMPZ location; where q is a proper look ahead to compensate for the phase distortion.

NMPZ close to the unit circle, the resulted phase would still be distorted but the phase distortion will be bounded within $\pm 90^o$ as shown in Figure 5.5.

5.3.1.3 Direct Inversion

As shown in the previous subsections, ZPETC approximate the inverse of unstable zeros by sacrificing the magnitude while ZMETC only considers the magnitude during inversion. In this section, a direct inversion which approximates the inversion of unstable zeros while taking both phase and magnitude into consideration is introduced.

The inversion of the stable closed-loop system G is not realizable because of the non-minimum phase zeros become unstable filter after inversion. Therefore, different methods are used to approximate the dynamic response of the system

inversion. For any given stable system G, the transfer function can be written as in Equation 5.8 where non-minimum phase zeros are grouped together as $B^-(z^{-1})$. The direct inversion filter of system G can be written as,

$$G^{-1}(z) = \frac{A(z)}{B^+(z)} \underbrace{\frac{1}{B^-(z)}}_{\text{unstable filter}} \tag{5.17}$$

which is an unstable filter caused by the inversion of the non-minimum phase zeros.

Instead of inverting the non-minimum phase zeros directly, the approximated direct inversion method first uses a Finite Impulse Response(FIR) filter to approximate the dynamic response of the filter as,

$$B^-_{FIR}(z^{-1}) \approx B^-(z^{-1}) \tag{5.18}$$

Then the approximated direct inversion filter can be denoted as,

$$F_{di}(z) = z^{d-n_{di}} \underbrace{\frac{A(z^{-1})}{B^+(z^{-1})}}_{\text{IIR}} \underbrace{\frac{1}{B^-_{FIR}(z^{-1})}}_{\text{FIR}} \tag{5.19}$$

And the overall transfer function will be,

$$F_{di}(z)G(z) = z^{-n_{di}} \frac{B^-(z^{-1})}{B^-_{FIR}(z^{-1})} \tag{5.20}$$

where n_{di} is the length of the FIR filter.

Both of the phase and magnitude are being taken care of in the approximated direct inversion method, but $B^-_{FIR}(z^{-1})$ is the truncated approximation of $B^-(z^{-1})$, the overall transfer function is not exactly unity across all frequencies. The performance of the approximated direct inversion can be improved by increasing the length of the FIR filter. While increasing the filter length will also increase the necessary preview length of the overall system which could not be

realizable in some cases. Fortunately, ILC algorithm executes the control update law off-line which allows very long preview length to the system.

5.3.2 Data Based

5.3.2.1 Time reversal phase cancellation

In section 5.3.1.1, the zero-phase compensation is made by taking the complex conjugate of the unstable zeros $B^-(z^{-1})$ which mirrors the unstable zeros into the unit circle. While cascade the filter with it's own complex conjugate pair, the resulted phase becomes zero across all frequency. Instead of taking the complex conjugate of the unstable zeros $B^-(z^{-1})$, the same zero phase effect can be achieved by forward-backward filtering [Gus96].

Consider a bounded signal $u(t)$ with z transform $U(z)$ filtered through a stable linear system $G(z)$ and define the resulting output $y(t)$ with $Y(z)$,

$$Y(z) = G(z)U(z) \tag{5.21}$$

then reverse the output $Y(z)$ and feed it through the linear system again,

$$Y_2(z) = G(z)G^*(z)U^*(z) \tag{5.22}$$

so if $U^*(z)$ is chosen to be the tracking reference $R(z)$, then zero phase filtering is achieved.

5.3.2.2 FFT inversion

The proposed frequency inversion method uses the step signal as the input to excite the system dynamic. Since an impulse may not have enough energy to excite all the system states, the average step response data will be a better candidate to approximate the ideal impulse signal. The main idea is to approximate the system by using a truncated impulse response. And then the inversion is happened in frequency domain.

In discrete time domain, the impulse is defined as,

$$\delta[n] = \begin{cases} 0, & n \neq 0 \\ 1, & n = 0 \end{cases} \tag{5.23}$$

and a step function can be represented as,

$$1[n] = \begin{cases} 0, & n < 0 \\ 1, & n \geq 0 \end{cases} \tag{5.24}$$

From Equation 5.23 and 5.24, the impulse can be decomposed into the the combination of two step functions start from different time. And the two step functions are shifted from another, we can further find the transfer function between a step function and the impulse as,

$$\begin{aligned} \delta[n] &= 1[n] - 1[n-1] \\ &= \frac{z-1}{z}\, 1[n] \end{aligned} \tag{5.25}$$

For a linear time invariant system, the approximated impulse response can be obtained by filtering the step response data through filter $\frac{z-1}{z}$ as shown in Equation 5.25.

The resulted impulse response, $h(n)$, characterizes the system dynamic. The Fast Fourier Transform will be applied to $h(n)$ to obtain the frequency response of the system. But proper signal processing techniques have to be considered to avoid the pitfalls in the FFT [GH80]. In order to avoid the spreading of energy from one frequency into adjacent ones, or leakage, Blackman-Harris window function is applied to system impulse response as,

$$h_w(n) = h(n)w(n) \tag{5.26}$$

and proper length of zero padding is added to the end of $h_w(n)$ to increase the number of points to 2048.

The corresponding frequency domain representation is found using the Fourier transform of the windowed impulse response

$$H_w(n) = \sum_{k=0}^{N-1} h_w(k) e^{-j2\pi nk/N} \tag{5.27}$$

where $H_w(n)$ is the Fourier coefficients of the windowed impulse response.

The evaluation of inverting system frequency response can be obtained by,

$$H_w^{-1} = (1, \ldots, 1) \oslash (H_w(0), \ldots, H_w(N-1)) \tag{5.28}$$

However, for well-behaved closed-loop system, the frequency response roll-off above the system bandwidth which makes $H_w(n)$ have components close to 0 at high frequency. In addition, the non-minimum phase zero in the system will also cause the magnitude of $H_w(n)$ approaches zero at the frequency of the unstable zero. The element-wise division will be dividing complex numbers closed to zero which ends up with a high gain in the inversion filter. In order to get around this issue, a reference model is used to evaluate the system inversion.

Since the system dynamic roll-off above the system bandwidth, a low-pass filter with cut-off frequency around system bandwidth is served as the model for employing inversion. The frequency response of the low-pass filter, $Q(n)$, can be obtained by following the aforementioned process.

Instead of inverting the system dynamics by itself, the proposed frequency inversion method obtained the system dynamic inversion with the low-pass filter as,

$$F_{fi}(n) = (Q(0), \ldots, Q(N-1)) \oslash (H_w(0), \ldots, H_w(N-1)) \tag{5.29}$$

so that the evaluation of the dynamic inversion, F_{fi}, will not be dividing by numbers close to zero.

The impulse response of the dynamic inversion filter can be obtained by applying Inverse Fourier transform

$$f_{fi}(n) = \sum_{k=0}^{N-1} F_{fi}(k) e^{j2\pi nk/N} \tag{5.30}$$

where $f_{fi}(n)$ is a finite impulse response with number of points at 2048, and the inversion filter can be constructed as,

$$F_{fi}(z^{-1}) = \sum_{k=0}^{n} f_{fi}(k) z^{-k} \tag{5.31}$$

The group delay of F_{fi} is determined by the delay of the low-pass filter. If the low-pass filter is chosen to be a linear phase filter, the group delay of the proposed frequency inversion filter, F_{fi}, can be compensated by adding proper steps of look-ahead.

5.4 Simulation Results

5.4.1 Modeling of Linear Motor

In order to demonstrate the proposed methods along with other popular inversion methods, a linear motor was used as the plant for a control experiment. The system is composed of a linear motor, an Aerotech BA-50 amplifier with bandwidth at 2 kHz, and a real-time desktop target equipped with National Instruments PCIe-7841R FPGA board was serving as the real-time controller.

Figure 5.6 shows the 4^{th} order curve fit of the model compared to the actual frequency response. The low-order model is obtained by fitting a forth-order polynomial curve to the frequency response of closed-loop system with sampling

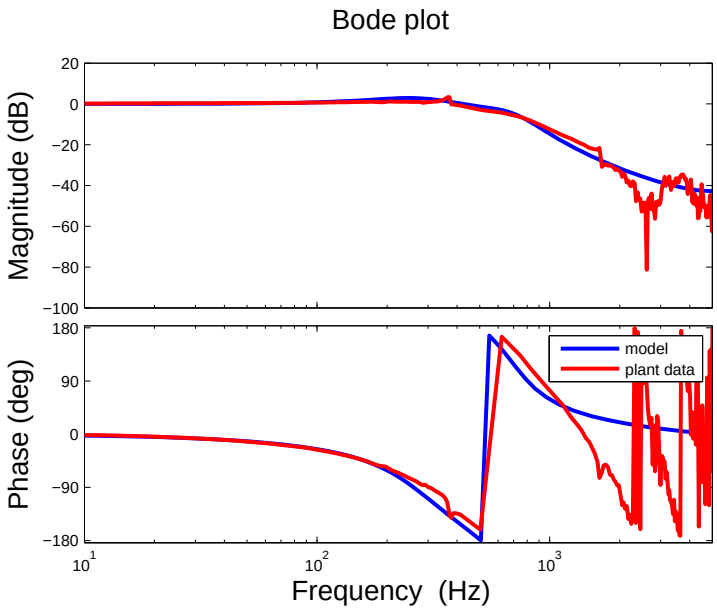

Figure 5.6: Frequency response of the stable closed-loop system. Blue: 4^{th} order curve fit model; Red: Frequency response data. The bandwidth of the closed-loop system is at 500 Hz

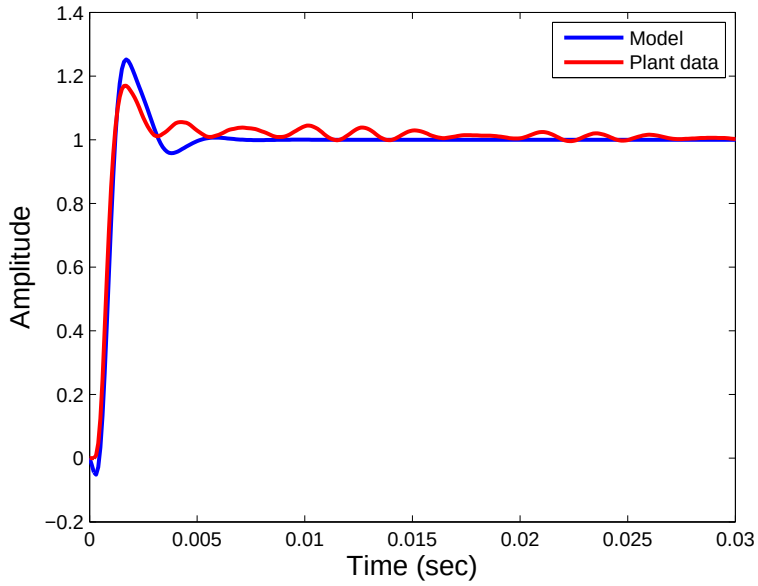

Figure 5.7: Step response of the 4^{th} order model and experimental data. Blue: 4^{th} order model; Red: experimental data.

rate at 10 kHz, and the resulted 4^{th} order model of the discrete time closed-loop system is

$$G(z) = \frac{-0.02(z - 1.664)(z - 0.648)(z + 0.036)}{(z^2 - 1.804z + 0.835)(z^2 - 1.599z + 0.764)} \tag{5.32}$$

and there is one unstable zero at $z = 1.664$.

Figure 5.7 shows the comparison of step response for the low order model and experimental data. The low order model captures the trend of the experimental data, but it does not include the high frequency oscillation exists in the experimental data.

In order to increase the system robustness, a linear phase low-pass Q-filter is added into the ILC update law as shown in equation 5.3. The cut-off frequency of the Q-filter is chosen to be the bandwidth of the system dynamic, so that the learning function can be turned off at high frequency region to avoid picking up

noise in learning function.

The Q-filter is designed as a linear phase moving average filter

$$Q(z, z^{-1}) = \frac{\sum_{i=0}^{m} a_i z^i + \sum_{i=1}^{m} a_i z^{-i}}{2\sum_{i=1}^{m} a_i + a_0} \tag{5.33}$$

where a_i are the filter coefficients to be designed and the filter length is $2m$.

5.4.2 ILC with ZPETC

By applying the Zero Phase inversion technique in Equation 5.10 to the 4^{th} order discrete model in Equation 5.32, the zero phase error tracking controller, F_{zp} can be obtained.

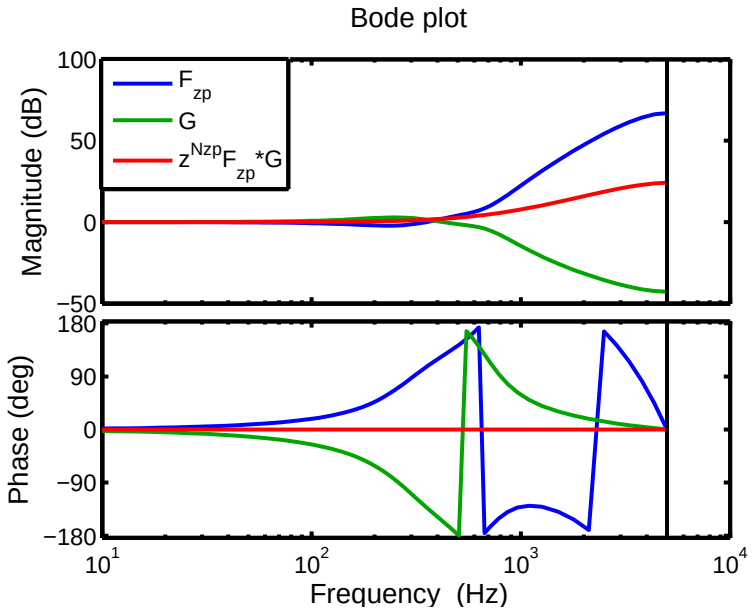

Figure 5.8: Frequency response of the Zero-Phase error tracking controller, F_{zp}, pre-stabilized closed system G, and the compensated transfer function $z^{nu+d}F_{zp}G$

Figure 5.8 shows the frequency response of the zero-phase error tracking controller, the closed-loop system dynamics, and the closed-loop system with zero-phase feed-forward controller. The frequency response of $F_{zp}G$ shows that ZPETC

is very close to the system inversion at low frequency. But the magnitude increases as frequency goes higher.

Since the 4^{th} order discrete model has a non-minimum phase zero at $z = 1.6$, the zero-phase inversion technique will create magnitude distortion at high frequency region. According to section 5.3.1.1, while the non-minimum phase zero is at $z = 1.6$ the magnitude at nyquist frequency would be around 50 dB. Therefore, the frequency response of the overall system will have magnitude greater than 0 dB at high frequency region which is vulnerable to noise and model uncertainty. In order to increase the robustness and maintain system stability at high frequency, a linear phase low -pass filter would be cascaded with the zero-phase error tracking controller.

5.4.3 ILC with ZMETC

The zero-magnitude error tracking controller can be obtained by applying Equation 5.14 to the 4^{th} order discrete model. And the frequency response of the zero-magnitude error tracking controller, closed loop system, and the overall transfer function is shown in Figure 5.9.

Since the low-order model has a non-minimum phase zero near the unit circle. According to the analysis in 5.3.1.2, the phase distortion can be attenuated by applying one-step look ahead to the zero-magnitude error tracking controller.

5.4.4 ILC with Direct Inversion

The direct inversion method approximates the unstable non-minimum phase inversion by a finite impulse response filter. Therefore, the filter length will affect the performance of the inversion filter. Although longer filter length can have better performance, it also needs more computation power to implement. Besides, the effectiveness of the improvement in increasing the filter length will be less

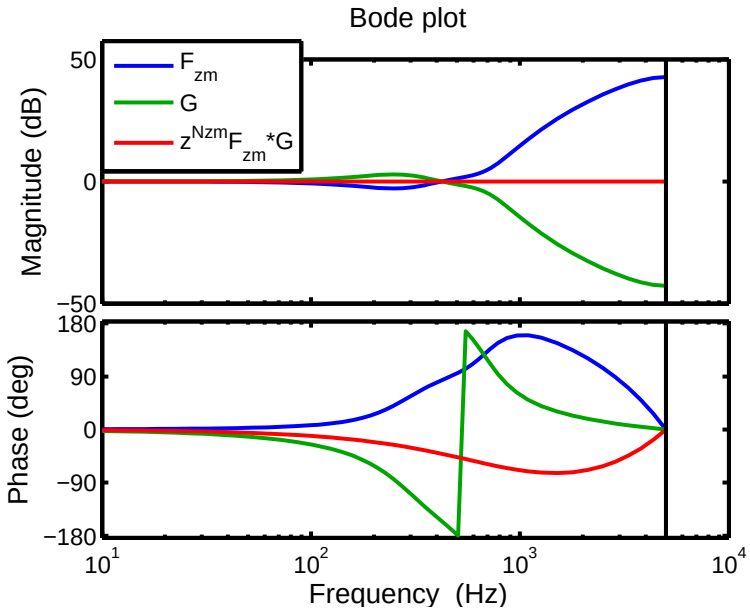

Figure 5.9: Frequency response of the Zero-Magnitude error tracking controller, F_{zm}, G, and the compensated transfer function, $z^{d+1}F_{zm}G$

significant while the filter length reaches certain number.

While a 45^{th} order finite impulse response filter is used to approximate the non-minimum phase zero at $z = 1.6$, the norm of $z^q - GF_{di}$ is at -190 dB which means the approximated inversion is very close to the inverse of the low-order model.

Figure 5.10 shows the frequency response of the 45^{th} order approximated direct inversion filter, the closed-loop system G, and the overall transfer function. Although the filter length is longer than either ZPETC or ZMETC, direct inversion is able to compensate for magnitude and phase at the same time providing almost perfect inversion across all frequencies. Since it is an anti-causal filter, proper preview steps is required in the implementation. It might be applicable for some cases that preview step is limited, since the ILC update law is executed off-line, we can always have enough preview steps by padding zeros at the beginning and

the end of the data vectors.

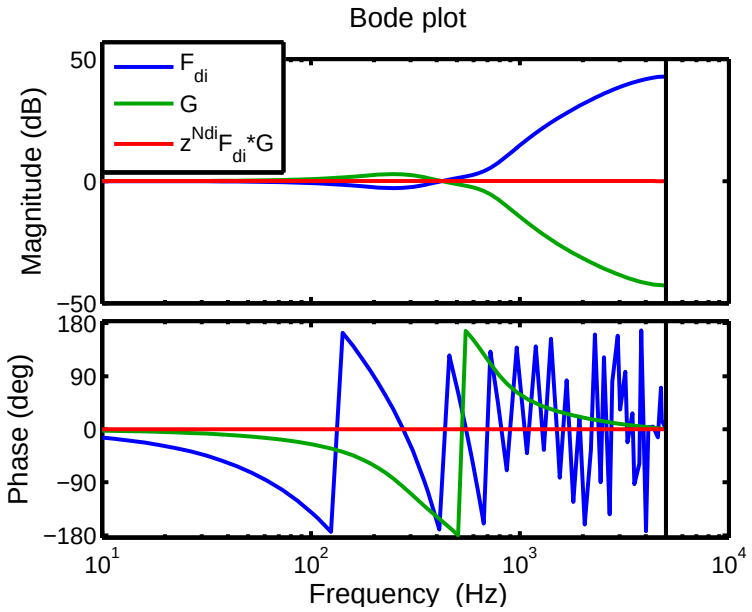

Figure 5.10: Frequency response of the Approximated Direct Inversion, F_{di}, the pre-stabilized system G, and the compensated transfer function

5.4.5 ILC with FFT Inversion

Figure 5.11 shows the frequency response of the proposed frequency inversion filter, the closed-loop system dynamic, and the overall transfer function. Since the proposed frequency inversion method does not use low-order model to construct the inversion filter, it does not have either zero phase or zero magnitude compensation to the low order model. In addition, the use of reference model in the proposed frequency inversion causes the compensated transfer function rolls-off at 500 Hz. However, the low order model does not capture all the system dynamics, the proposed frequency domain inversion is expected to perform better in implementation. This can be verified by looking at the evaluation of Equation 5.34 with high order model, and the comparison will be presented in the next section.

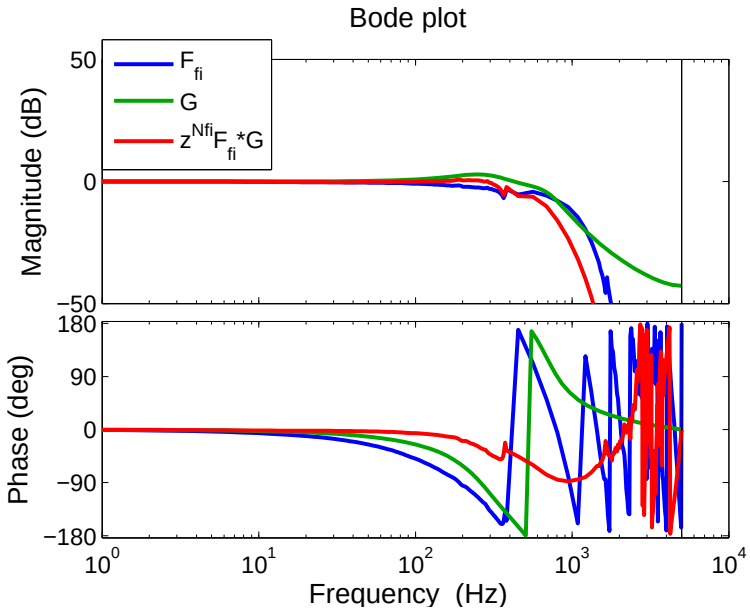

Figure 5.11: Frequency response of the proposed frequency inversion filter, F_{fi} and the closed-loop system dynamic

5.4.6 Sufficient Stability Condition

In order to increase robustness and guarantee system stability, the linear phase low-pass filter, Q which is also the reference model for the proposed frequency inversion method, is used in the ILC update law as shown in Equation 5.3.

In Equation 5.4, the sufficient stability condition for the inversion based ILC algorithm is derived as,

$$|Q(z) - Q(z)F_x(z)G(z)| < 1 \tag{5.34}$$

where $F_x(z)$ stands for different inversion method.

Figure 5.12 shows the frequency response of Equation 5.34 for different inversion methods with 4^{th} order model. Since direct inversion has almost perfect inversion across all frequencies, $|Q(z) - Q(z)F_{di}(z)G(z)| = |Q(z)(1 - F_{di}(z)G(z))| = 0$ is expected while G is the low order model in the evaluation.

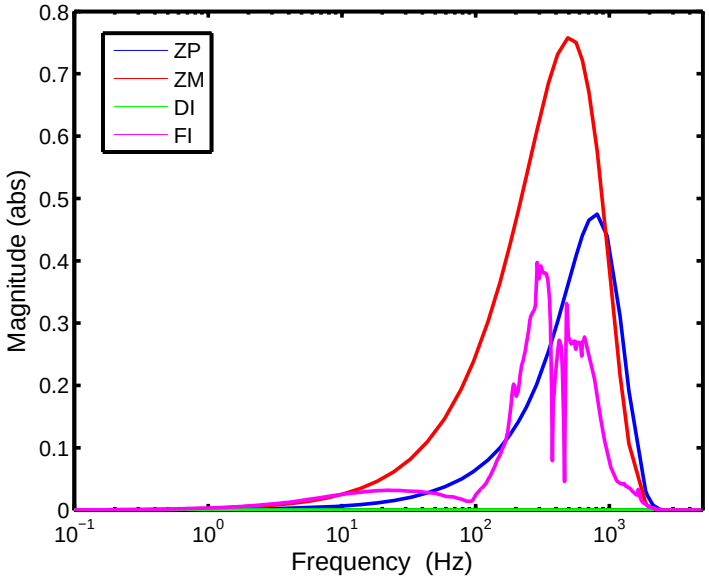

Figure 5.12: Magnitude of $|Q(z) - Q(z)F_x(z)G(z)|$ for different inversion methods.

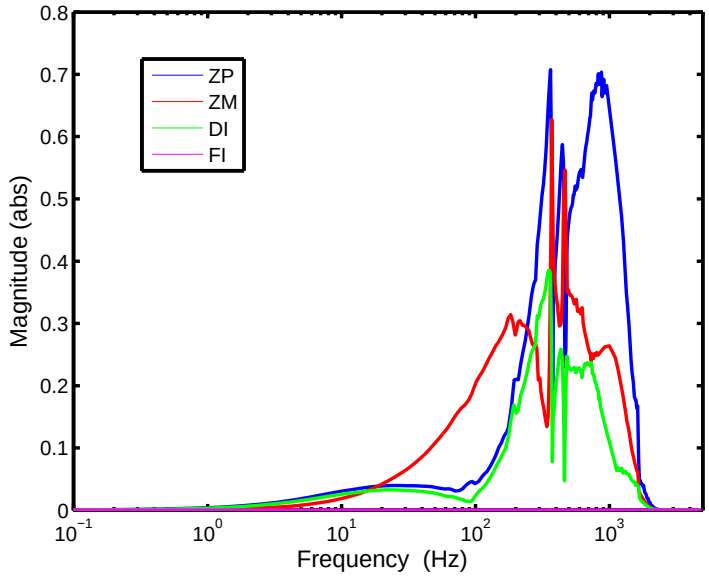

Figure 5.13: Magnitude of $|Q(z) - Q(z)F_x(z)G_{high}(z)|$ for different inversion methods.

Figure 5.13 shows the frequency response of Equation 5.34 for different inversion methods with high order model. Since the proposed frequency domain inversion uses the data to construct the inversion filter, $|Q(z) - Q(z)F_{fi}(z)G(z)| = |Q(z)(1 - F_{di}(z)G(z))| \approx 0$ is expected while G is the high order model in the evaluation.

Because the proposed frequency inversion method is designed based on the information from experimental data, it does not suffer from unmodelled dynamic. Other methods may have pretty good approximated inversion with respect to the low-order model, the unmodelled dynamic introduce some distortion in both magnitude and phase.

5.4.7 Results Comparison

5.4.7.1 Piston profile

In this section, the simulation result of different inversion method in tracking a non-circular piston profile is presented. Figure 5.14 shows the tracking reference used in the simulation.

Figure 5.15 shows the Root-Mean-Square (RMS) error for different inversion methods while tracking 50 Hz triangular profile. A Q-filter with cut-off frequency at 500 Hz is used for all inversion methods. The converged error for all methods are around 0.5 μm, while the FFT inversion method reaches the converged error within one iteration.

5.4.7.2 Triangular profile

In this section, the simulation result of different inversion method in tracking a 50 Hz triangular profile is presented. Figure 5.16 shows the tracking reference used in the simulation.

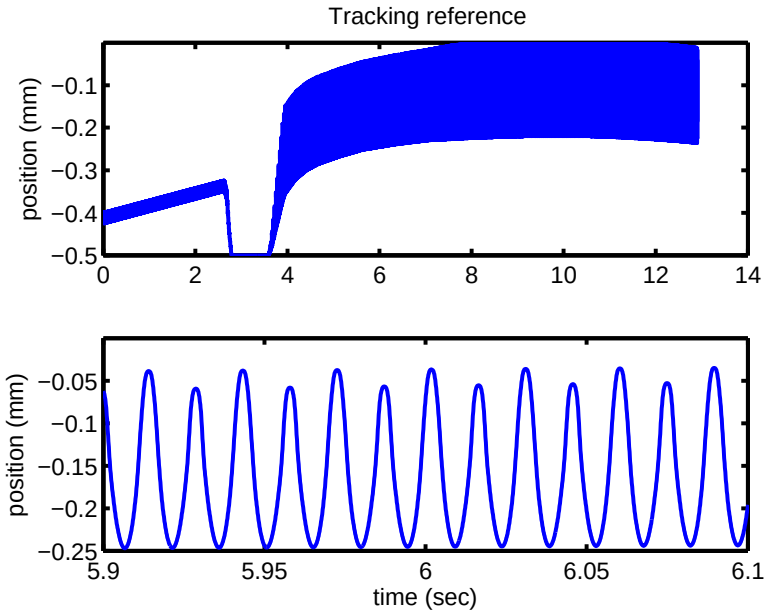

Figure 5.14: Non-circular piston profile

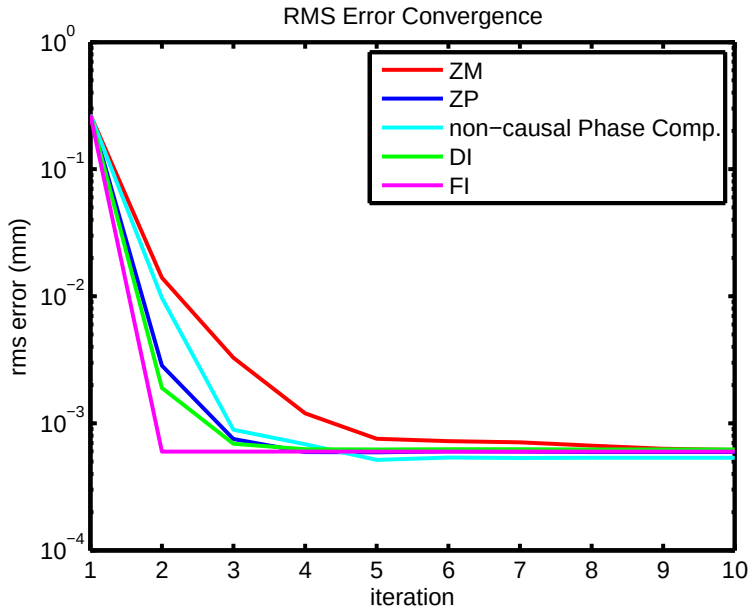

Figure 5.15: RMS error at different iteration for tracking non-circular piston profile

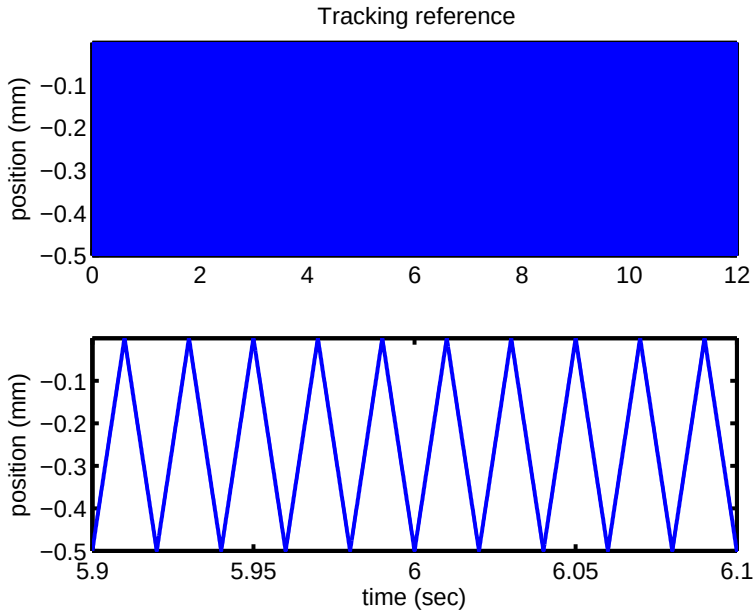

Figure 5.16: 50 Hz triangular profile

Figure 5.17 shows the Root-Mean-Square (RMS) error for different inversion methods while tracking 50 Hz triangular profile. A Q-filter with cut-off frequency at 500 Hz is used for all inversion methods. The converged error for all methods are around 1.4 μm, while the FFT inversion method reaches the converged error within one iteration.

5.5 Experimental Results

5.5.1 Piston Profile

Figure 5.18 shows the RMS error convergence for different learning functions. The proposed FFT inversion method has the lowest RMS error at iteration one, meaning the inversion is more accurate than the others. Non-causal phase compensation seems to suffer from the noise/disturbances in implementation, causing the RMS error starts to diverge after 6 iterations. According to the stability analysis shown

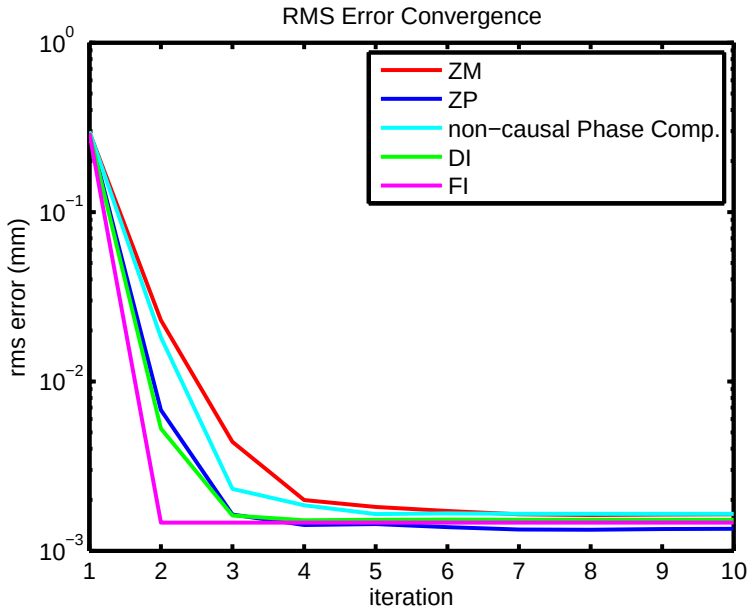

Figure 5.17: RMS error at different iteration for tracking 50 Hz triangular profile

in Figure 5.13, ZPETC has two peaks at high frequency region which leads ILC with ZPETC to be not asymptotically stable. Therefore, we had to lower the cut-off frequency of the Q-filter from 500Hz to 350Hz to have a asymptotically stable system. According to Equation 5.5, this will increase the asymptotic error in the sense that the controller is "turned off" above 350Hz compared to 500Hz for other learning functions.

Because of the proposed frequency inversion method uses the experimental data to construct the inversion filter, it has better knowledge about the actual system dynamics. A higher bandwidth Q-filter can be used without violating the sufficient stability condition in Equation 5.34. Therefore, the proposed frequency inversion filter with Q cuts-off at 1000Hz was implemented and the asymptotic error is further reduced to 0.18 μm. As for the other learning functions, the final RMS error converge to around 0.5 μm.

The final converged error and the corresponding iteration of different learning

function are listed in table 5.1.

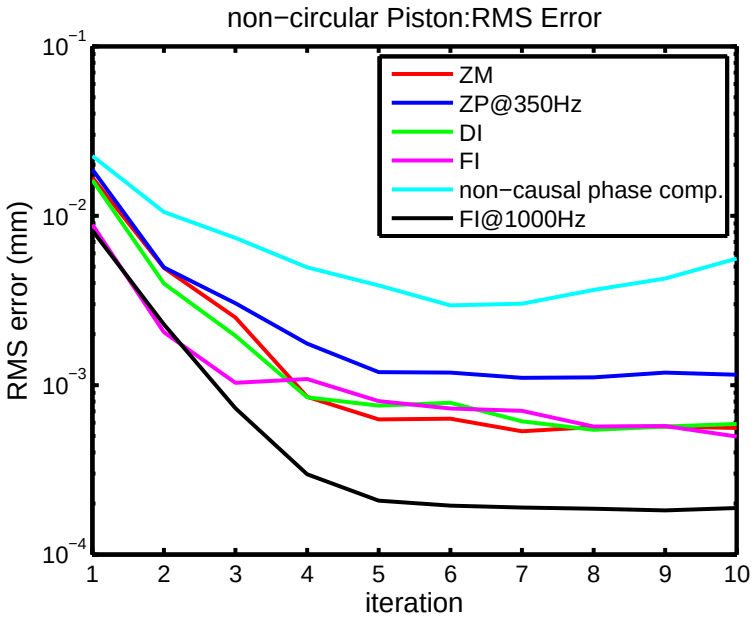

Figure 5.18: Piston profile: RMS error at different iterations.

In Figure 5.20, the linear motor output position of different learning function at four different location of the non-circular profile is presented. The non-causal phase compensation method has significant overshoots while the tracking reference changes direction. The ZMETC, direct inversion, and the proposed frequency inversion method have the best performance, the linear motor output position is almost on top of the tracking reference.

5.5.2 Triangular Profile

Figure 5.21 shows the RMS error convergence for different learning functions. The proposed FFT inversion method has the fastest convergence rate, meaning the inversion is more accurate than the others. Non-causal phase compensation seems to suffer from the noise/disturbances in implementation, causing the RMS error starts to diverge after 7 iterations. According to the stability analysis shown

	RMS error (μm)
ZP (Q@350Hz)	1.1
ZM	0.53
DI	0.54
FI	0.49
FI (Q@1000Hz)	0.18
phase cancel.	2.95

Table 5.1: The converged RMS error of different learning function for non-circular piston profile

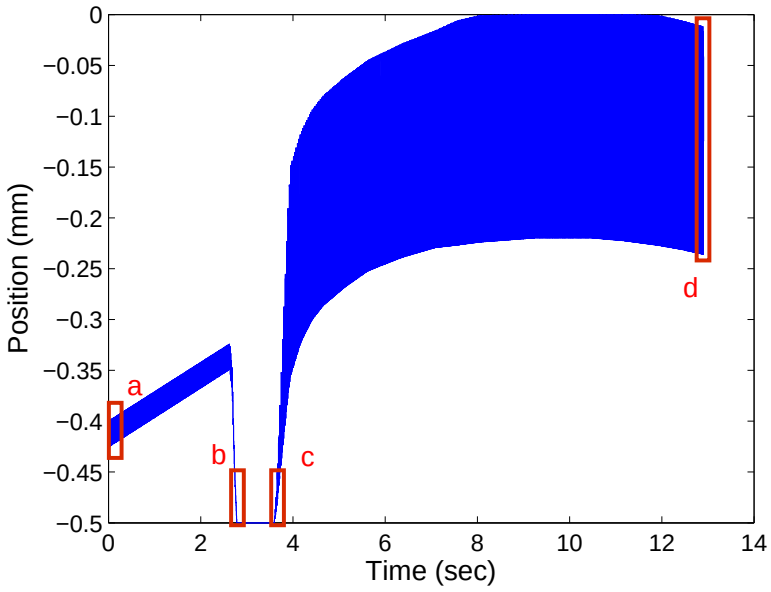

Figure 5.19: Time trace plot of non-circular piston profile

in Figure 5.13, ZPETC has two peaks at high frequency region which decrease the tracking performance. As for the other learning functions, the final RMS error converge to around 1.3 μm.

The final converged error and the corresponding iteration of different learning

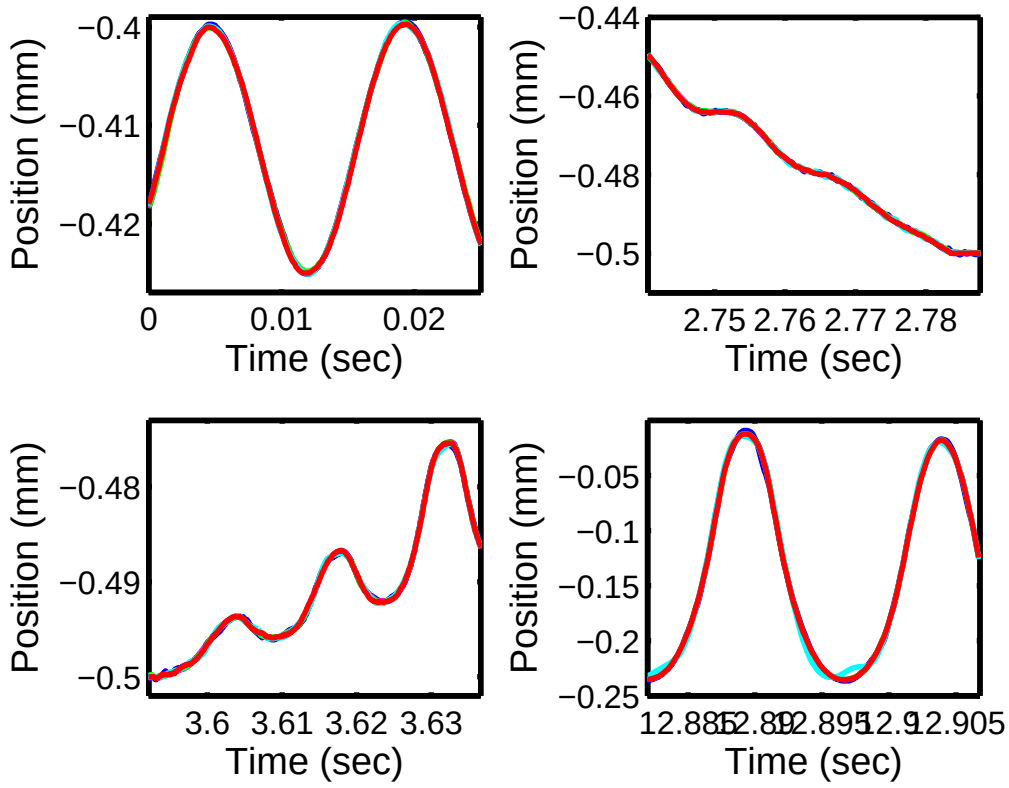

Figure 5.20: Time trace plot of different learning function for 4 different part of non-circular piston profile;

function are listed in table 5.2.

In Figure 5.22, the linear motor output position of different learning function within two period of 50Hz triangular profile is presented. The non-causal phase compensation method has significant overshoots before and after the tracking reference changes direction. The ZMETC, direct inversion, and the proposed frequency inversion method have the best performance, the maximum tracking error is within $\pm$ 10 μm.

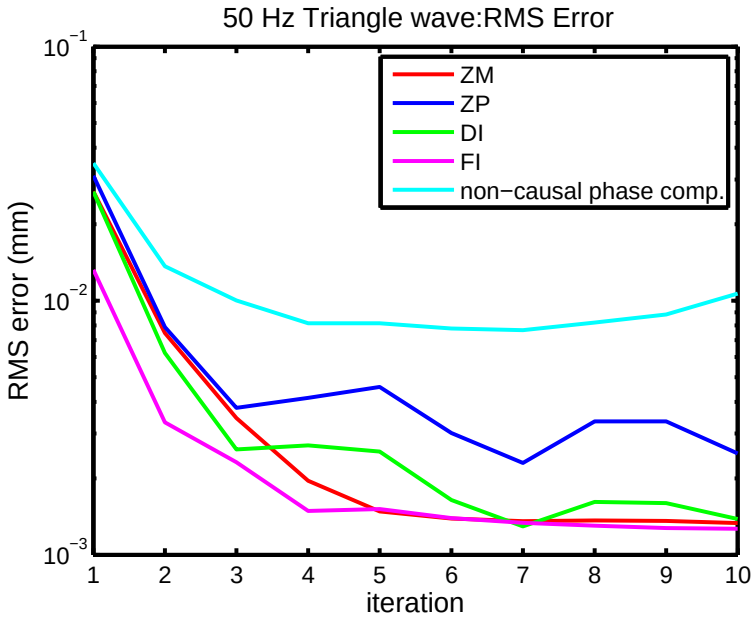

Figure 5.21: Triangular profile: RMS tracking error at different iterations.

5.6 Application to Machining

In the previous sections, the performance of different inversion-based ILC algorithm has been presented in simulation and experiment. However, the motivation of this research is to improve the machining performance by using iterative learning control.

We implemented the ILC with ZPETC to a Computer-numerical-control lathe for machining a non-circular piston profile. The piston profile shown in Figure 5.19 is used in the machining process. The machining conditions are:

- Spindle speed: 3000 RPM
- Feedrate: 0.4 mm/rev

Figure 5.23 shows the tracking error of machining a non circular piston profile. The tacking error is within $\pm$ 10μm. It is evident that the tracking error has an offset towards the negative direction. The negative direction corresponds to the

	RMS error (μm)
ZP (Q@350Hz)	2.29
ZM	1.33
DI	1.29
FI	1.26
phase cancel.	7.64

Table 5.2: The converged RMS error of different learning function for triangular profile

tool tip on the CNC lathe, meaning the cutting force causes extra error while actual machining. The RMS value of the tracking error shown in Figure 5.23 is 1.83 μm compared to 1.1 μm without cutting force.

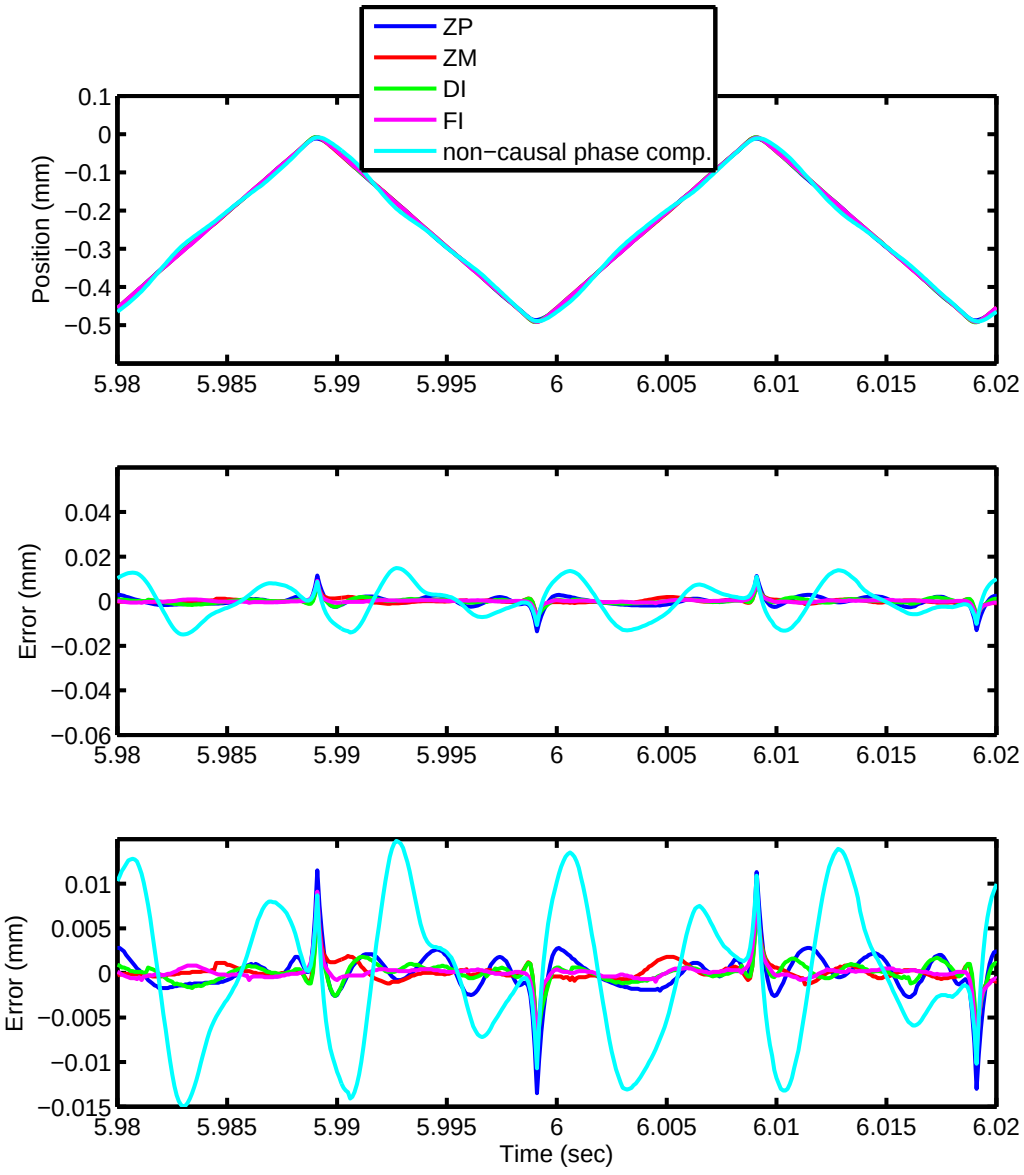

Figure 5.22: Time trace plot of different learning function for tracking a 50Hz triangular profile;

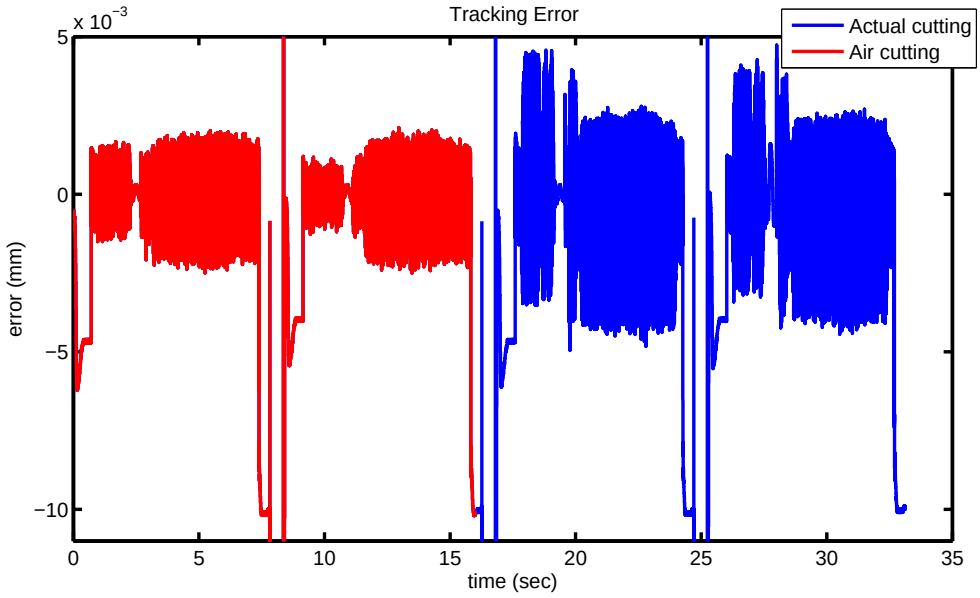

Figure 5.23: Tracking error while actual cutting

CHAPTER 6

Conclusion

In this dissertation the repetitive and iterative learning control for power converters and precision motion control has bee discussed. The typical PI controlled power converters can not guarantee zero steady state error while tracking AC quantities. Although PI control in DQ coordinate provides zero steady state error, it does not compensate for other harmonics. Because of the power converters become MIMO system in DQ coordinate, it adds difficulties in designing advanced controllers to compensate for harmonics.

In Chapter 2, the repetitive control for MIMO system is introduced. By using the Smith-McMillan decomposition, the ZPETC for MIMO systems can be formulated. The decoupled compensated I/O map enables the repetitive control design for MIMO systems.

Implementing control within DQ rotating frame is able further improve the overall performance, it not only enhances the tracking of 60Hz AC voltage but also adds more compensation to the harmonics. In either fixed frame or DQ rotating coordinate, repetitive control is able to compensate the harmonics components to a very small extent with THD around 0.1%. Although the MIMO repetitive control does not have significant improvement over SISO repetitive control for power inverter, it could be beneficial for other applications where the control can only be design for MIMO system.

The proposed repetitive control for MIMO system in Chapter 2 enables the design of repetitive control for power converters in DQ coordinate. In chapter 4,

we have shown that the Repetitive control in DQ coordinate for power rectifier has superior performance with THD = 0.006% corresponds to almost 100% in power conversion without considering switching loss, heat loss, and etc.

In chapter 5, a detail analysis and derivation of different non-minimum phase dynamic inversion methods including ZPETC, ZMETC, direct inversion, and the proposed data-based frequency domain inversion is presented. Although the proposed data-based frequency inversion method requires the implementation of high order filter, it is able to provide the exact frequency response as designed. The simulation and experimental results both show that the proposed frequency inversion method has the best performance among others. Because of the highly accurate inversion, it has the fastest convergence rate with the smallest converged error.

References

[ACM07] Hyo-Sung Ahn, YangQuan Chen, and Kevin L Moore. "Iterative learning control: brief survey and categorization." *IEEE TRANSACTIONS ON SYSTEMS MAN AND CYBERNETICS PART C APPLICATIONS AND REVIEWS*, **37**(6):1099, 2007.

[Age12] International Energy Agency. "2012 Key World Energy Statistics." *http://www.iea.org/publications/freepublications/publication/kwes.pdf*, 2012.

[Ari90] Suguru Arimoto. "Learning control theory for robotic motion." *International Journal of Adaptive Control and Signal Processing*, **4**(6):543–564, 1990.

[BA08] Kira L Barton and Andrew G Alleyne. "A cross-coupled iterative learning control design for precision motion control." *Control Systems Technology, IEEE Transactions on*, **16**(6):1218–1231, 2008.

[BK04] Giuseppe S Buja and Marian P Kazmierkowski. "Direct torque control of PWM inverter-fed AC motors-a survey." *Industrial Electronics, IEEE Transactions on*, **51**(4):744–757, 2004.

[BTA06] Douglas A Bristow, Marina Tharayil, and Andrew G Alleyne. "A survey of iterative learning control." *Control Systems, IEEE*, **26**(3):96–114, 2006.

[CGF04] Ramon Costa-Castelló, Robert Grinó, and Enric Fossas. "Odd-harmonic digital repetitive control of a single-phase current active filter." *Power Electronics, IEEE Transactions on*, **19**(4):1060–1068, 2004.

[CL96] Chiang-Ju Chien and Jing-Sin Liu. "A P-type iterative learning controller for robust output tracking of nonlinear time-varying systems." *International Journal of Control*, **64**(2):319–334, 1996.

[CM02] Yang Quan Chen and Kevin L Moore. "An optimal design of PD-type iterative learning control with monotonic convergence." In *Intelligent Control, 2002. Proceedings of the 2002 IEEE International Symposium on*, pp. 55–60. IEEE, 2002.

[CMS02] Martina Calais, Johanna Myrzik, Ted Spooner, and Vassilios G Agelidis. "Inverters for single-phase grid connected photovoltaic systems-an overview." In *Power Electronics Specialists Conference, 2002. pesc 02. 2002 IEEE 33rd Annual*, volume 4, pp. 1995–2000. IEEE, 2002.

[CMY06] Yang Quan Chen, Kevin L Moore, Jie Yu, and Tao Zhang. "Iterative learning control and repetitive control in hard disk drive industry-a tutorial." In *Decision and Control, 2006 45th IEEE Conference on*, pp. 2338–2351. IEEE, 2006.

[CN09] CM Colson and MH Nehrir. "A review of challenges to real-time power management of microgrids." In *Power & Energy Society General Meeting, 2009. PES'09. IEEE*, pp. 1–8. IEEE, 2009.

[CQL04] Insik Chin, S Joe Qin, Kwang S Lee, and Moonki Cho. "A two-stage iterative learning control technique combined with real-time feedback for independent disturbance rejection." *Automatica*, **40**(11):1913–1922, 2004.

[CT13] Herrick L Chang and Tsu-Chin Tsao. "An efficient fixed-point realization of inversion based repetitive control." In *American Control Conference (ACC), 2013*, pp. 5948–5953. IEEE, 2013.

[CT14] Herrick L Chang and Tsu-Chin Tsao. "High-Sampling Rate Dynamic InversionFilter Realization and Applications in Digital Control." *Mechatronics, IEEE/ASME Transactions on*, **19**(1):238–248, 2014.

[DB00] Dick De Roover and Okko H Bosgra. "Synthesis of robust multivariable iterative learning controllers with application to a wafer stage motion system." *International Journal of Control*, **73**(10):968–979, 2000.

[F I93] I F II. "IEEE recommended practices and requirements for harmonic control in electrical power systems." 1993.

[FW76] Bruce A Francis and W Murray Wonham. "The internal model principle of control theory." *Automatica*, **12**(5):457–465, 1976.

[GH80] Adly A Girgis and Fredric M Ham. "A quantitative study of pitfalls in the FFT." *Aerospace and Electronic Systems, IEEE Transactions on*, (4):434–439, 1980.

[GN01] Svante Gunnarsson and Mikael Norrlöf. "On the design of ILC algorithms using optimization." *Automatica*, **37**(12):2011–2016, 2001.

[Gus96] Fredrik Gustafsson. "Determining the initial states in forward-backward filtering." *IEEE Transactions on Signal Processing*, **44**(4):988–992, 1996.

[HNA10] Makoto Hagiwara, Kazutoshi Nishimura, and Hirofumi Akagi. "A medium-voltage motor drive with a modular multilevel PWM inverter." *Power Electronics, IEEE Transactions on*, **25**(7):1786–1799, 2010.

[KK96] Dong-Il Kim and Sungkwun Kim. "An iterative learning control method with application for CNC machine tools." *Industry Applications, IEEE Transactions on*, **32**(1):66–72, 1996.

[KPB05] Soeren Baekhoej Kjaer, John K Pedersen, and Frede Blaabjerg. "A review of single-phase grid-connected inverters for photovoltaic modules." *Industry Applications, IEEE Transactions on*, **41**(5):1292–1306, 2005.

[KT04] K Krishnamoorthy and Tsu-Chin Tsao. "Repetitive Learning Control for Precision Machining of Complex Profiles." In *ASME 2004 International Mechanical Engineering Congress and Exposition*, pp. 63–69. American Society of Mechanical Engineers, 2004.

[KT14a] Christopher Kang and Tsu-Chin Tsao. "Control of Magnetic Bearings with plug-in time-varying harmonic resonators." In *American Control Conference (ACC), 2014*, pp. 4237–4242. IEEE, 2014.

[KT14b] K Krishnamoorthy and Tsu-Chin Tsao. "Design and Implementation of Repetitive Control based Noncausal Zero-Phase Iterative Learning Control." *arXiv preprint arXiv:1408.2490*, 2014.

[KZ08] Kyong-Soo Kim and Qingze Zou. "Model-less inversion-based iterative control for output tracking: piezo actuator example." In *American Control Conference, 2008*, pp. 2710–2715. IEEE, 2008.

[Mac89] Jan Marian Maciejowski. "Multivariable feedback design." *Electronic Systems Engineering Series, Wokingham, England: Addison-Wesley,—c1989*, **1**, 1989.

[NG02] Mikael Norrlöf and Svante Gunnarsson. "Time and frequency domain convergence properties in iterative learning control." *International Journal of Control*, **75**(14):1114–1126, 2002.

[RBB07] Arman Roshan, Rolando Burgos, Andrew C Baisden, Fred Wang, and Dushan Boroyevich. "A DQ frame controller for a full-bridge single phase inverter used in small distributed power generation systems." In *Applied Power Electronics Conference, APEC 2007-Twenty Second Annual IEEE*, pp. 641–647. IEEE, 2007.

[RBL97] Michael J Ryan, William E Brumsickle, and Robert D Lorenz. "Control topology options for single-phase UPS inverters." *Industry Applications, IEEE Transactions on*, **33**(2):493–501, 1997.

[RPL09] Brian P Rigney, Lucy Y Pao, and Dale A Lawrence. "Nonminimum phase dynamic inversion for settle time applications." *Control Systems Technology, IEEE Transactions on*, **17**(5):989–1005, 2009.

[Saa94] Samer S Saab. "On the P-type learning control." *Automatic Control, IEEE Transactions on*, **39**(11):2298–2302, 1994.

[SAG04] J Salaet, S Alepuz, A Gilabert, and J Bordonau. "Comparison between two methods of DQ transformation for single phase converters control. Application to a 3-level boost rectifier." In *Power Electronics Specialists Conference, 2004. PESC 04. 2004 IEEE 35th Annual*, volume 1, pp. 214–220. IEEE, 2004.

[SMS03] Makoto Saitou, Nobuyuki Matsui, and Toshihisa Shimizu. "A control strategy of single-phase active filter using a novel dq transformation." In *Industry Applications Conference, 2003. 38th IAS Annual Meeting. Conference Record of the*, volume 2, pp. 1222–1227. IEEE, 2003.

[SO91] Toshiharu Sugie and Toshiro Ono. "An iterative learning control law for dynamical systems." *Automatica*, **27**(4):729–732, 1991.

[SSC03] Bhim Singh, Brij N Singh, Ambrish Chandra, Kamal Al-Haddad, Ashish Pandey, and Dwarka P Kothari. "A review of single-phase improved power quality AC-DC converters." *Industrial Electronics, IEEE Transactions on*, **50**(5):962–981, 2003.

[SSP03] VB Sriram, Sabyasachi SenGupta, and Amit Patra. "Indirect current control of a single-phase voltage-sourced boost-type bridge converter operated in the rectifier mode." *Power Electronics, IEEE Transactions on*, **18**(5):1130–1137, 2003.

[Tay04] Abdelhamid Tayebi. "Adaptive iterative learning control for robot manipulators." *Automatica*, **40**(7):1195–1203, 2004.

[Tom87] Masayoshi Tomizuka. "Zero phase error tracking algorithm for digital control." *Journal of Dynamic Systems, Measurement, and Control*, **109**(1):65–68, 1987.

[Tsa88] Tsu-Chin Tsao. *Digital Tracking Control And Its Application to Noncircular Machining*. PhD thesis, University of California, Berkeley, 1988.

[TT87] Tsu-Chin Tsao and Masayoshi Tomizuka. "Adaptive zero phase error tracking algorithm for digital control." *Journal of dynamic systems, measurement, and control*, **109**(4):349–354, 1987.

[TT94] Tsu-Chin Tsao and Masayoshi Tomizuka. "Robust adaptive and repetitive digital tracking control and application to a hydraulic servo for noncircular machining." *Journal of dynamic systems, measurement, and control*, **116**(1):24–32, 1994.

[TTC89] Masayoshi Tomizuka, Tsu-Chin Tsao, and Kok-Kia Chew. "Analysis and synthesis of discrete-time repetitive controllers." *Journal of Dynamic Systems, Measurement, and Control*, **111**(3):353–358, 1989.

[WCT09] Yigang Wang, Kevin C Chu, and Tsu-Chin Tsao. "An analysis and synthesis of internal model principle type controllers." In *American Control Conference, 2009. ACC'09.*, pp. 488–493. IEEE, 2009.

[ZCS02] Richard Zhang, Mark Cardinal, Paul Szczesny, and Mark Dame. "A grid simulator with control of single-phase power converters in DQ rotating frame." In *Power Electronics Specialists Conference, 2002. pesc 02. 2002 IEEE 33rd Annual*, volume 3, pp. 1431–1436. IEEE, 2002.

[ZH03] Daniel Nahum Zmood and Donald Grahame Holmes. "Stationary frame current regulation of PWM inverters with zero steady-state error." *Power Electronics, IEEE Transactions on*, **18**(3):814–822, 2003.